Deal Alexandra Michelle (Orcid ID: 0000-0002-1540-9277)
Frandsen Benjamin Normann (Orcid ID: 0000-0002-9211-3939)
Vaida Veronica (Orcid ID: 0000-0001-5863-8056)

Lactic Acid Photochemistry Following Excitation of S_0 to S_1 at 220 to 250 nm

Deal, Alexandra M.[†]; Frandsen, Benjamin N.[†]; Vaida, Veronica[†]*

*Corresponding Author; Email: vaida@colorado.edu; Phone: 303-492-8605
[†] Department of Chemistry and Cooperative Institute for Research in Environmental Sciences, University of Colorado Boulder, Boulder, Colorado 80309, United States

Keywords: Multiphase Photochemistry, Carboxylic Acids, Isotopic Studies, Decarboxylation, Aqueous Photochemistry, Conformer Specific Reactivity, Ab-Initio Calculations

Full Abstract

Lactic acid, a small α-hydroxy acid, is a multifunctional molecule that is prevalent on modern Earth and found in abiotic environments. Recently, there has been interest in the photochemistry of carboxylic acids in general. Specifically, the photochemistry of lactic acid, due to its prevalence and functionality, has garnered attention by the biomass valorization and abiotic chemistry communities. However, aqueous lactic acid photochemistry studies are limited, and gas-phase lactic acid photolysis had not been performed. This work combines theory and experiments to explore the gas-phase and aqueous phase photochemistry of lactic acid following excitation of S_0 to S_1 at 220 – 250 nm. We find that lactic acid primarily photodecomposes via decarboxylation in both phases. In the gas phase, secondary chemistry leads to mainly CO_2 and CO, while in the aqueous phase, subsequent radical chemistry leads to a variety of products with one to four carbons. Isotopic substitutions, including the use of ^{13}C tagged lactic acid and using D_2O as a solvent, are used to infer mechanistic pathways for the major photolysis products. Computation shows that individual conformers may contribute to the overall photochemistry to a different degree than their relative abundance would suggest. The identified products and proposed mechanisms shown here serve to illustrate the photochemistry of lactic acid in the presence of high energy ultraviolet radiation. This knowledge may aid process and catalyst design for biomass valorization/organic synthesis and may provide insight into abiotic chemistry in environments exposed to high energy ultraviolet radiation.

Short Abstract

Theory and experiments are used to explore the gas and aqueous phase photochemistry of lactic acid following excitation of S_0 to S_1 at 220 – 250 nm. Lactic acid is shown to

This is the author manuscript accepted for publication and has undergone full peer review but has not been through the copyediting, typesetting, pagination and proofreading process, which may lead to differences between this version and the Version of Record. Please cite this article as doi: 10.1002/poc.4316

primarily photodecompose via decarboxylation. While gas-phase photochemistry leads to mainly CO_2 and CO, aqueous phase photochemistry leads to a variety of products with 1 to 4 carbons. Isotopic substitutions, including ^{13}C tagged lactic acid and D_2O solvation, are used to infer mechanistic pathways for the major photolysis products.

TOC Figure

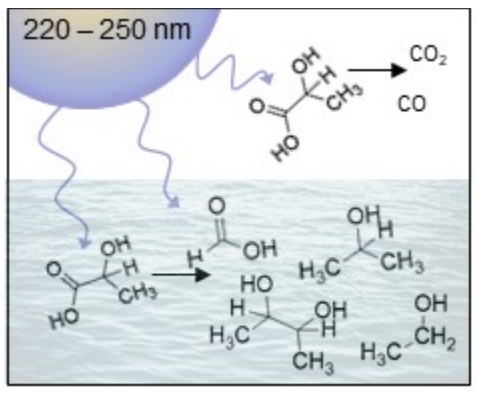

Introduction

Lactic acid, and lactic acid photolysis, has recently garnered attention among both the abiotic chemistry[1] and biomass valorization research communities[2]. As well as being the product of metabolic cycles in modern life, lactic acid has been found in meteorites[3] and can be formed by the photolysis of pyruvic acid[4] indicating its potential role in abiotic chemistry[5]. It has recently gained recognition as a potential precursor to depsipeptides and primitive enclosures, both of which could contribute to the formation of life.[1a, 1b]

Additionally, lactic acid, having both a hydroxyl and a carboxylic acid functional group, has been described as a "commodity chemical sleeping giant" for biomass valorization[2b-d]. With the increasing cost of using fossil fuels for energy, plastics, etc., research communities are actively seeking methods for processing natural molecules to form practical chemicals capable of replacing certain fossil fuel functionalities. Lactic acid, which is readily available in the contemporary Earth environment[6], has gained interest as a potential feedstock. It can be inexpensively produced by biomass fermentation or catalysis[2b, 2e], but further processing to make functional molecules such as ethanol[7] or 2,3-butanediol[8] remains challenging. Recently, photochemistry using high energy ultraviolet radiation has been investigated as a method for processing lactic acid, but research into the photochemical mechanisms and byproducts, which could aid in process or catalyst design, is still ongoing[2a, 2g].

Understanding the photochemistry of lactic acid is also important for abiotic chemistry as many abiotic environments such as early Earth and exoplanets are, or would have been, exposed to high energy ultraviolet radiation. On early Earth, for example, during the Hadean period with the absence of oxygen and ozone, radiation with higher energy ($\lambda > 190$ nm) would have reached Earth's surface[9]. In some cases, ultraviolet radiation can form complex molecules from simple organic monomers[5b]. In the case of aqueous pyruvic acid photochemistry, for example, radical species are formed which then abstract hydrogen and/or recombine to form an array of complex, higher molecular weight species[1e, 4, 10]. The end products of such photolysis reactions are highly dependent on both the reactant molecule and its environment,[4, 10a, 11] hence it is important to understand lactic acid photolysis mechanisms, accurately determine the end products, and determine any differences due to the environment.

It is well established that carboxylic acids in general have a $n_O \rightarrow \pi_{CO}^*$ transition which is excited around $\lambda = 200$ nm ($E = 6.2$ eV)[12]. Upon excitation of this transition, multiple carboxylates including lactate (deprotonated lactic acid) have been shown to decarboxylate *via* the short-lived lowest singlet excited state[12a, 13]. Over the last hundred years, it has been shown that the main products from the high energy photolysis of aqueous lactic acid in an anoxic environment are ethanol and CO_2, suggesting lactic acid dissociates by decarboxylation as its primary photolysis mechanism[2a, 14].

In this study, we investigate the photochemistry of lactic acid following excitation of S_0 to S_1 at 220 to 250 nm using isotopic labeling in different environments. In addition to aqueous photolysis, which has been previously studied[2a, 14], the gas-phase photolysis of lactic acid is explored to determine multiphase effects on final products and mechanisms. We also use isotopic substitution to extrapolate mechanistic pathways. Specifically, we use ^{13}C-tagged lactic acid to determine the fate of the carboxylic acid carbon from both gas-phase and aqueous photolysis and we replace H_2O with D_2O in a subset of aqueous experiments to explore the role of the solvent as a potential reactant in aqueous photolysis.

Experimental observations are bolstered using theory in this work. Lactic acid is known to have seven conformers in the gas phase[15]: here we extend the study of lactic acid conformers in the aqueous phase. To this end we use density functional theory, coupled cluster, and complete basis set methods to explore bond enthalpies and ground state and excited state geometries/energies for lactic acid conformers in both gas and aqueous phases. Overall, the multiphase photochemistry of lactic acid is investigated using both experiment and computation.

Methods

Experimental

All experiments used solid L-lactic acid (MP Biomedicals, >98% purity) except for carbon isotope experiments which used solid L-lactic acid-1-^{13}C (Sigma Aldrich, >99% atom ^{13}C), see SI for structure. Both isotopologues were checked for purity using ^{1}H NMR prior to photolysis and found to contain no significant impurities, see SI. Solutions were made with Milli-Q water (18.2 MΩ; 3 ppb TOC) or deuterium oxide (Cambridge Isotope Laboratories, 99.9% atom D).

UV Absorption Spectrum

Lactic acid was diluted with Milli-Q (MQ) water to a final concentration of ~10 mM to avoid non-linear absorption effects. A laser-driven light source (Energetiq EQ-99) was collimated using a parabolic mirror, passed through a Horiba iHR-550 spectrometer using the 600 l/mm grating, and collected by a charged coupled device (Horiba Synapse). The CCD was operated in position mode set to λ = 220 nm which provides data between λ = 180-260 nm. A clean 10 mm quartz cuvette was placed in the beam path. A background was taken of MQ water, the water was replaced by the lactic acid solution, and the wavelength-dependent intensity of photons passing through the sample was collected. Both background and sample signals were baseline corrected for noise and an absorption spectrum was calculated.

Photolysis Source

The photolysis source used in all experiments was a 1000 W Xe(Hg) lamp (Newport 6293) with an attached water filter (Newport 6123NS) to reduce infrared radiation from reaching the sample. The lamp was affixed with the standard quartz lenses and the water filter was affixed with quartz windows. The light source emittance after attenuation by the water filter and a quartz window was measured using the Horiba iHR-550 spectrometer and attached charged coupled device (Horiba Synapse).

FTIR Product Analysis

Gas-phase species in all experiments were monitored by Fourier transform infrared spectroscopy (FTIR) utilizing the external beam of a Bruker IFS 66v/s which was collected by a liquid nitrogen cooled MCT detector, as described previously[16]. The Bruker consists of a Globar mid-IR light source, KBr beam splitter, and KBr exit window. Reaction cells were equipped with CaF_2 windows in the IR beam path. Prior to photolysis, spectra were collected for 30 minutes monitoring CO_2 and H_2O signals to probe for and

subsequently eliminate leaks into the reaction cell. After photolysis was started spectra were recorded approximately every 15 minutes.

Spectra were later analyzed using a combined visual and mathematical approach. They were first visually compared with available standards to determine the presence or absence of expected or possible product molecules. Once the component product molecules were identified, concentration trends were determined using the MATLAB software described previously, ANIR, which was developed at CEAM (Spain)[10b, 16]. Briefly, this software uses a linear square fitting routine with a modified filtering process which removes baseline abnormalities and broad absorptions of unknown compounds. This software compares each experimental spectrum against a set of standardized spectra. Standardized spectra use the same apodization function (Happ-Genzel) and resolution (0.5 cm^{-1}) as experimental spectra. HITRAN data was used in cases when an experimental standardized spectrum could not be found. References using HITRAN data[17] were constructed with a MATLAB program that applies a Lorentzian lineshape to each transition using the provided spectral line intensity, S_{ij} [cm^{-1}/(molecule*cm^2)], and self-broadened half width half max, γ_{self} [cm^{-1}/atm]. Reference spectra were generated with a resolution to match experimental spectra and adjusted to account for natural isotopic abundance. Note that the spectra generated from HITRAN data are not degraded by an apodization function and the fit performed by ANIR will thus have some intrinsic error. In general, concentrations of gas-phase species reported in this work are qualitative and should be viewed only as an assessment of relative trends for product species.

An FTIR spectrum of ^{13}C-tagged lactic acid was also taken as a reference, see SI, using the same method as described previously for obtaining the untagged lactic acid FTIR spectrum[15a].

Gas-phase Photolysis

Gas-phase photolysis experiments using L-lactic acid or isotopically labelled lactic acid, L-lactic acid-1-^{13}C, were performed in a specially designed glass cell as shown in Figure 1 and described previously[16]**.** This cell has an IR beam path length of 60 cm and photolysis beam path of 50 cm. The cell has a CaF_2 window at each end in the IR beam path and a quartz window at each end in the photolysis beam path. Areas between the spectrometer exit window, photochemical cell, and MCT detector were enclosed in a plastic casing and purged with CO_2-scrubbed, dry air to minimize the interference of atmospheric CO_2 and H_2O on the FTIR measurements. The solid lactic acid sample, ~0.5 g, was placed in a round bottom flask attached to the photochemical cell with a valve. Pressure was monitored by a 10 Torr Baratron absolute pressure transducer located between the cell and the manifold. Prior to photolysis, the cell and sample were evacuated to ~400 mTorr to remove O_2, water, and volatile impurities. The cell was then closed to

the vacuum pump and the lactic acid sample allowed to equilibrate in the evacuated cell overnight. No large leaks were detected. At the beginning of the experiment, the valve to the solid sample was closed and the FTIR background spectrum was recorded. The photochemical cell was then exposed to the photolysis lamp and reactions were allowed to continue until product concentrations began to plateau, usually 5-6 hours. FTIR spectra were recorded every 15 minutes during photolysis and analyzed as described above. The experiment was run multiple times, when possible, to ensure reproducible results.

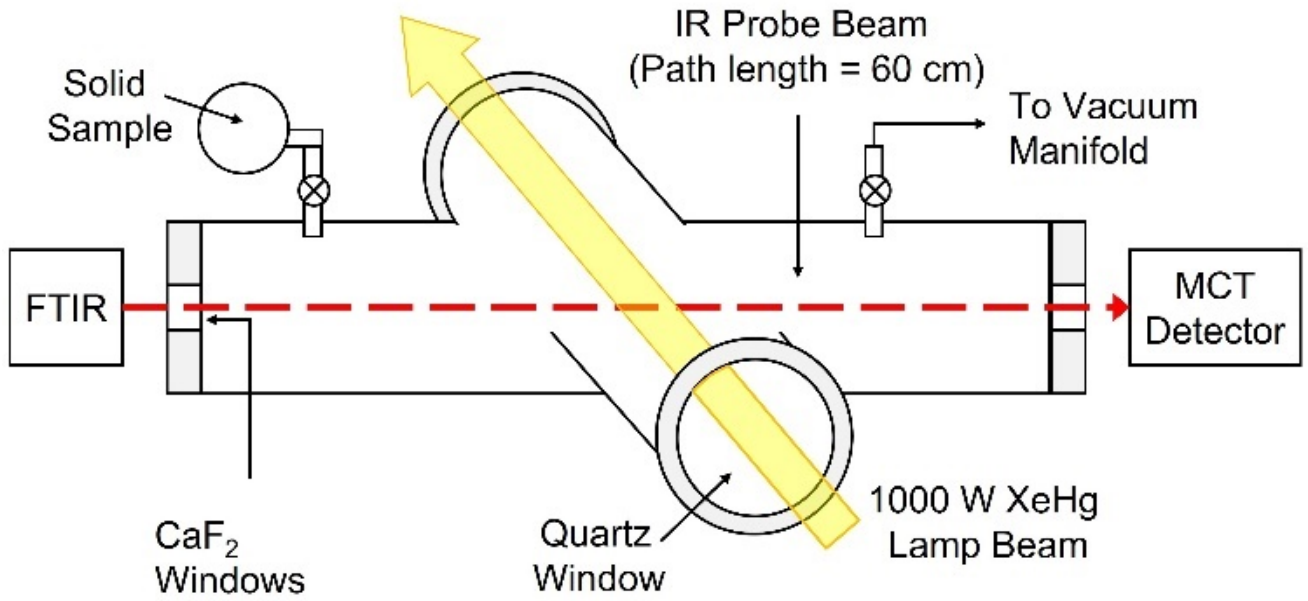

Figure 1: Experimental set up for gas-phase photolysis.

Gas-phase photolysis was also investigated using intermittent and limited exposure to the photolysis light source to rule out any dark or thermal chemistry and assess wall effects, similar to a previous study on pyruvic acid[16]. A pyrex filter was used to remove high energy photons when testing for visible light-induced and/or thermal chemistry that may have been caused by the photolysis lamp. First, lactic acid was kept in the absence of irradiation for 45 minutes while spectra were recorded. Then the photolysis cell was exposed to the lamp in alternating intervals of only lower energy radiation (pyrex filter, $\lambda \geq 280$ nm) and the full lamp spectrum (no pyrex filter, $\lambda \geq 220$ nm). Results are shown in Figure 2.

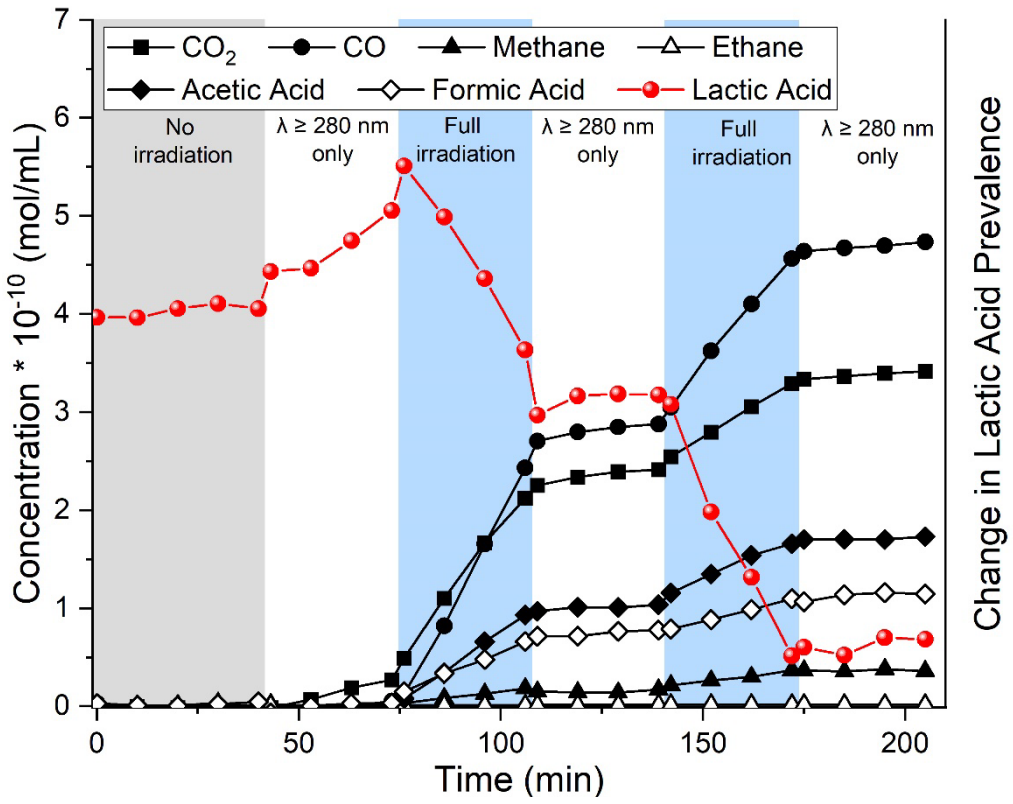

Figure 2: Representative gas-phase product FTIR trends for cycled photolysis experiments. The photolysis cell was first monitored with no irradiation (grey bar) and then cycled between periods of partial irradiation (using only photons with λ ≥ 280 nm, white bars) and periods of full irradiation (blue bars). The portions of the graph related to each period are denoted near the top. No significant changes were observed in the absence of irradiation or with photons of λ ≥ 280 nm.

Product species concentrations are not significantly affected by the absence of irradiation (grey bar) or during partial irradiation (λ ≥ 280 nm, white bars). Small increases during partial irradiation (λ ≥ 280 nm, blue bars) are likely due to species dislodging from the wall due to heating but are unlikely to impact overall photochemical trends. Dark chemistry, thermal chemistry, and wall effects are therefore negligible in this study.

Aqueous Photolysis

Aqueous phase photolysis experiments using L-lactic acid or isotopically labelled lactic acid, L-lactic acid-1-^{13}C, were performed in a specially designed glass cell as shown in Figure 3, using a set-up modified from previous studies[1e, 10b, 16]. This cell has an IR

beam path length of 50 cm, and the photolysis beam directly contacts the aqueous sample. The cell has a CaF_2 window at each end in the IR beam path. Areas between the spectrometer exit window, photochemical cell, and MCT detector were enclosed in a plastic casing and purged with CO_2-scrubbed, dry air to minimize the interference of atmospheric CO_2 and H_2O on the FTIR measurements. Solution samples were placed in the bottom of the cell. The photolysis beam was directed downwards by a UV-rated mirror and passes through a quartz window to enter the photolysis cell. Solutions of both labelled and unlabeled lactic acid were diluted with MQ water to a concentration of 100 mM. Additionally, one set of experiments diluted non-isotopically labelled lactic acid with D_2O. A temperature probe was affixed to the bottom of the photochemical cell and the sample area was immersed in a cold-water bath set to 15 °C. The average temperature measured by the probe was ~18 °C across all experiments despite some thermal energy provided by the Xe(Hg) lamp. Prior to photolysis, the cell and sample were evacuated to remove dissolved gases. The cell was then closed to the vacuum pump and the FTIR background spectrum was recorded. The photochemical cell was exposed to the photolysis lamp and reactions were allowed to continue for the desired time, typically ~4 hours. FTIR spectra were recorded every 15 minutes during photolysis and analyzed as described above. The experiments were run multiple times, when possible, to ensure reproducible results.

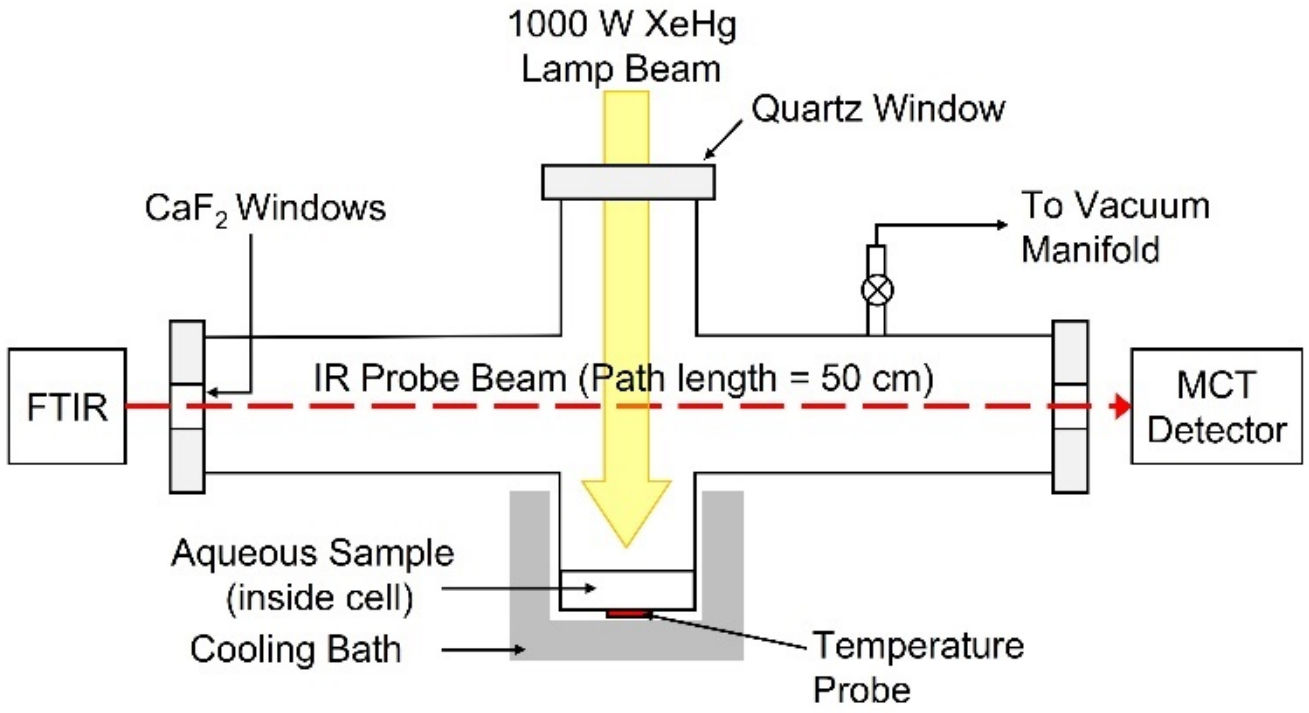

Figure 3: Experimental set-up for aqueous photochemical experiments.

NMR Product Analysis

^{1}H NMR spectra were taken before and after aqueous photolysis using a 300 MHz Bruker Fourier 300 spectrometer. Aqueous photolysis samples were prepared using 0.63 mL of the sample solution and 0.07 mL of D_2O, resulting in a 90%/10% H_2O/D_2O solvent mixture. For lactic acid in D_2O experiments, no additional solvent was added. Resultant spectra were analyzed using visual comparison with standards to determine the presence or absence of expected or possible product molecules. Once an initial determination was proposed, reference spectra were taken under the same conditions to confirm peak assignments. Finally, the water peak was suppressed when necessary and relative concentrations for each product were determined using MestReNova (Mestrelab Research, Version 12.0) peak integration values.

Theoretical Methods

Computational chemistry methods including density functional theory (DFT), coupled cluster (CC), and complete basis set (CBS) were utilized to support the experiments in this work. The CBS-QB3[18] method was employed to calculate bond dissociation enthalpies (BDEs) for lactic acid. The calculations were done without modification to default settings. DFT was used to identify minimum energy structures on the ground state and excited state potential energy surfaces. The ωB97X-D functional[19] was used in conjunction with the aug-cc-pVTZ basis set[20] to optimize ground states and to calculate harmonic frequencies of the ground state minima. TD-DFT[21] using the ωB97X-D functional[19] with aug-cc-pVTZ basis set[20] was also used to calculate vertical electronic excitation energies and oscillator strengths and optimization of excited state geometries to get adiabatic excitation energies. Note that in this work adiabatic excitation energies are given as zero-point vibrational corrected energies, while vertical excitation energies are purely electronic energies. For excited state geometry optimizations, the DFT calculations used the unrestricted Kohn-Sham approach. The ωB97X-D functional was chosen for its known positive performance in TD-DFT[22] calculations. Vertical excitation energy and oscillator strength calculations for aqueous lactic acid used TD-DFT with a Polarizable Continuum Model (PCM)[22] of water. Geometries were reoptimized using PCM, but calculations were otherwise performed in the same manner as the solvent free forms. Infrared spectral shifts due to isotopic labeling were determined using VPT2 calculations[23]. Geometry optimization was performed and VPT2 calculations at the B3LYP[24]/may-cc-pVTZ[20, 25] level of theory were completed as described previously[15a], see SI for further details.

The vertical excitation energy and oscillator strength of the S_0 to S_1 transition in solvent free lactic acid was also calculated using coupled cluster methods (EOM-CCSD[26]/6-311+G(d)[27] with the frozen core option) after the previously determined geometries were re-optimized at the CCSD/6-311+G(d) level of theory. Initial attempts involved using CCSD[28] with the aug-cc-pVTZ basis set, but this approach was computationally too expensive. The aug-cc-pVTZ and 6-311+G(d) basis sets are both triple zeta, polarized, and include diffuse functions. The main difference is in the amount of contracted basis functions included. For second row atoms, the 6-311+G(d) basis set includes one polarized basis function and two diffuse basis functions, while the aug-cc-pVTZ includes three polarized basis functions and four diffuse basis functions. Furthermore, the 6-311+G(d) does not include any diffuse basis functions on hydrogens, while the aug-cc-pVTZ basis set does. However, it has been reported that the aug-cc-pVTZ basis set does not provide any significant improvement in excited state calculations over other triple zeta basis sets with fewer polarization and diffuse basis set functions[29], making the 6-311+G(d) basis set adequate for the more computationally expensive calculations. DFT and CBS-QB3 calculations were performed using Gaussian 16, Revision A.03[30] and coupled cluster calculations were completed using CFOUR, version 2.1[31] with the added 6-311+G(d) basis set downloaded from the Basis Set Exchange[32]. Further calculation details such as convergence criteria and keywords used can be found in the SI.

Results and Discussion

Lactic Acid Ultraviolet Excitation

Computational chemistry has previously identified seven possible lactic acid conformers in the gas phase[15]. These conformers are shown in Figure 4.

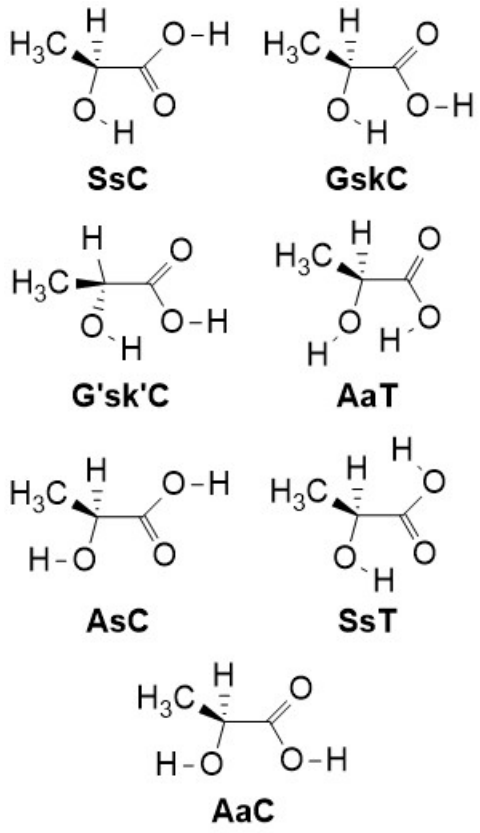

Figure 4: The seven identified lactic acid conformers; the shorthand naming convention follows that of previous literature.[15] Adapted from Frandsen et al.[15a].

Electronic transitions for each of these conformers were calculated to assess the conformer-specific relevance during photochemistry, both in gas phase and aqueous phase. For gas-phase calculations, the results from the AsC, SsT, and AaC conformers are omitted due to their low relative abundances (<0.1%).[15a] We report electronic transition calculations for the remaining four conformers (SsC, GskC, G'sk'C, and AaT) with two electronic structure methods, coupled cluster and density functional theory (DFT). The coupled cluster method, EOM-CCSD, is the higher-level method, but was not feasible to use for other calculations reported later in this work. Here, we use EOM-CCSD/6-311+G(d) to assess the DFT method, ωB97X-D/aug-cc-pVTZ, for further calculations. Relative abundances of the four most abundant conformers are given in Table 1 along with the calculated vertical excitation energies (VEEs) and oscillator strengths calculated by both methods. We see good agreement in the electronic transition energies and oscillator strengths across the two methods, raising confidence in the

computational results. There is also good agreement between the relative abundances calculated in this work and those determined by high-level calculations in previous work[15a].

Table 1 demonstrates that the SsC conformer has the highest relative abundance in the gas phase, but the GskC, G'sk'C, and AaT conformers all have lower energy $S_0 \rightarrow S_1$ transitions. The oscillator strengths between all conformers are comparable, excepting that of the G'sk'C conformer which is higher. Given that the actinic flux of our photolysis lamp has a much greater overlap with the lower energy transitions, discussed further below, lactic acid in a higher energy conformation (GskC, G'sk'C, or AaT) would likely be excited at a higher rate than that in the SsC conformation. The higher energy conformers may therefore contribute to gas-phase UV absorption and photochemistry more than their relative abundance would suggest.

The relative abundance of conformers and associated electronic transitions were also calculated for aqueous lactic acid using a PCM model, results in Table 2. These solvation results show a significant change in lactic acid conformer abundances and signify that all conformers may be relevant for aqueous chemistry. The significant changes in relative abundances for the AsC, SsT, and AaC conformers in the aqueous phase (each >1%) compared to the gas phase (each <0.1%) is attributed to hydrogen bonding with the solvent. As shown in Figure 1, the SsC, GskC, G'sk'C, AaT, and SsT conformers each have an internal hydrogen bond, while AsC and AaC conformers do not. This presence or lack of internal hydrogen bond largely dictates differences in the gas-phase conformational distribution. In the aqueous phase however, hydrogen bonding between lactic acid and water appears to reduce the importance of internal hydrogen bond differences allowing a greater conformational diversity than in the gas phase. This phenomenon has also been demonstrated for pyruvic acid, a similar molecule that also possesses a conformer-dependent internal hydrogen bond[10b].

The aqueous ultraviolet absorbance spectrum for ~10 mM lactic acid was recorded, and a synthetic spectrum based on the values reported in Table 2 was calculated. Both are shown in comparison with the recorded photolysis lamp actinic flux in Figure 5. The synthetic spectrum, black trace in Figure 5, considers the first four electronic transitions of each conformer, see SI for a full list of calculated transitions. Each transition was convoluted with a 0.7 eV full width at half maximum Gaussian function and weighted by the conformer aqueous relative abundance in Table 2. Note that the second, third, and fourth transitions in all conformers are most relevant for wavelengths below 200 nm and do not significantly contribute above 200 nm. Despite method limitations[33], we see that the synthetic spectrum, and thus the calculated transitions, are reasonably

accurate as the synthetic spectrum follows the shape of the experimental spectrum. This is especially true at wavelengths longer than 210 nm which encompasses the relevant photons in this study.

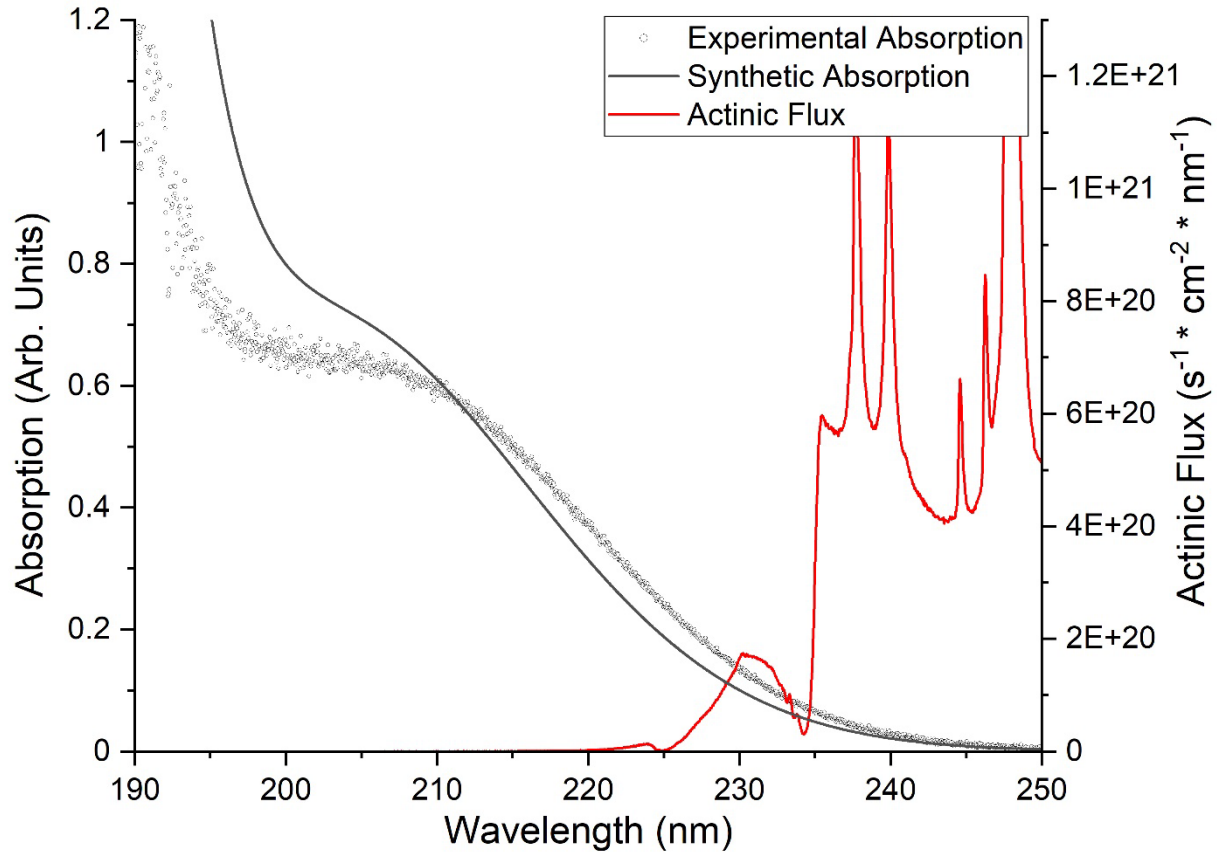

Figure 5: Aqueous lactic acid UV absorbance spectrum (black scatter, left y-axis) and synthetic lactic acid aqueous phase spectrum (black line, left y-axis, details in text). The experimental spectrum was obtained using a ~10 mM solution in a 1 cm cuvette. Both are compared with the photolysis lamp actinic flux output shown (red, right y-axis).

We use the calculated absorption cross sections and measured lamp actinic flux to calculate the conformer-specific excitation rates by the following equation:

$$\mathrm{ER} = \int_{\lambda_1}^{\lambda_2} w \cdot \sigma(\lambda) \cdot F(\lambda)\, d\lambda$$

Where ER is the excitation rate, w is a weighting factor set to the decimal version of the relative abundances given in Table 2, $\sigma(\lambda)$ is the absorption cross section, and $F(\lambda)$ is the actinic flux. The resulting ERs for each individual conformer were divided by the sum for all conformers, giving the relative ERs shown in Table 2. These results show that the VEE and oscillator strength significantly influences the absorption of each conformer. Specifically, the G'sk'C conformer stands out with an estimated ER% more than 5 times its relative abundance %, a phenomenon which arises due to its relatively low VEE and highest oscillator strength. Such differences could affect the photochemistry of lactic acid as different conformers may have different dissociation dynamics, though further assessment is beyond the scope of this work. It can be concluded, however, that the higher energy conformers of lactic acid in water contribute more to the photon absorption than their relative abundances would otherwise suggest and thus may contribute significantly to the overall photochemistry of lactic acid.

Gas-phase Photolysis

Gas-phase lactic acid was photolyzed in an anoxic environment and products were monitored *in-situ* by FTIR as described in Methods. Key regions of the resultant spectra showed CO_2, CO, acetic acid, formic acid, methane, and ethane formation, see SI. Once products were visually identified, the CEAM ANIR program was used to determine concentration trends over time. Representative product concentration trends are shown in Figure 6.

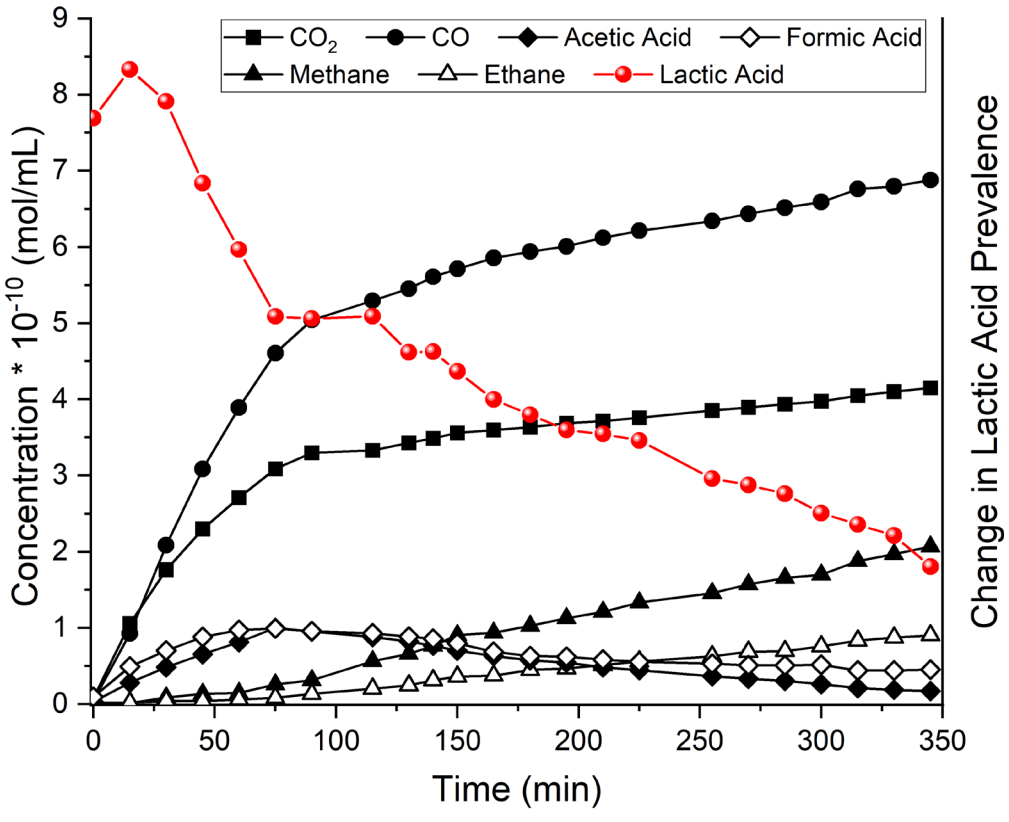

Notably, acetic acid[34] and formic acid[35] are themselves photoactive under these experimental conditions which explains their decline in concentration after ~1 hour of photolysis. They are known to produce CO_2, CO, water, and an array of radicals. Methane and ethane are also produced during lactic acid photolysis in small quantities and are likely secondary products given their delayed appearance.

Isotopically tagged lactic acid, with a ^{13}C located in the carboxyl group (structure shown in SI), was also photolyzed in the gas phase and monitored by FTIR as described in the Methods. A reference ^{13}C-tagged lactic acid spectrum was obtained, as described in Methods, to use when determining its change in prevalence. The spectrum, as shown

in SI, displayed a ~42 cm^{-1} redshift in the C=O stretch vibrational signal as compared to that of untagged lactic acid. The experimental spectra obtained during photolysis established $^{13}CO_2$ and ^{13}CO development in addition to the previously identified CO_2, CO, acetic acid, formic, acid, methane, and ethane formation. The $^{13}CO_2$ and ^{13}CO isotopologues are easily resolved from their CO_2 and CO counterparts by their spectral shifts; $^{13}CO_2$ features are 65 cm^{-1} lower in energy than CO_2 features and ^{13}CO features are 47 cm^{-1} lower than CO features[17]. The relevant portion of an example spectrum is shown in SI. Standard FTIR spectra for methane and ethane containing ^{13}C were compared with experimental spectra and neither species was identified as a photolysis product within the detection limits of our experiments[17, 36]. In the case of acetic acid and formic acid, we presume any isotopic carbon incorporation would take the primary location, within the carboxyl group. To the best of our knowledge, there are no available standards for acetic acid or formic acid containing ^{13}C, but VPT2 calculations on formic acid at the B3LYP/may-cc-pVTZ level with and without ^{13}C shows that the C=O fundamental vibrational transition would redshift by 39 cm^{-1}. Based on this calculation, we did not detect infrared signals indicative of acetic acid or formic acid containing ^{13}C. It is possible that each of these species is formed in a quantity below our detection limit, but we can conclude they are not major products.

Once products were visually identified, the CEAM ANIR program was again used to determine concentration changes. Representative product trends for ^{13}C-tagged lactic acid photolysis in the gas phase are shown in Figure 7.

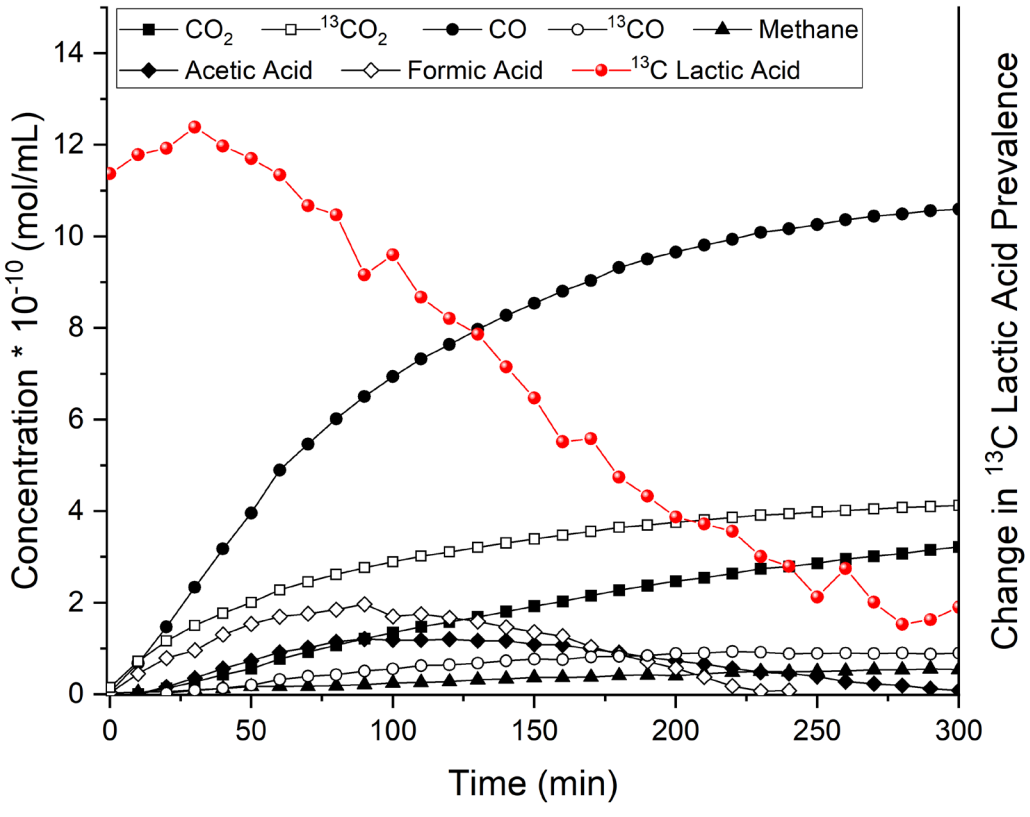

Figure 7: Representative product formation over time for ^{13}C-tagged lactic acid photolysis. The change in ^{13}C-tagged lactic acid prevalence (red, right y-axis) is relative; the scale is linear, but arbitrary with no defined zero. Concentrations of the products CO_2, $^{13}CO_2$, CO, ^{13}CO, formic acid, acetic acid, and methane are plotted against the left y-axis. No ^{13}C-tagged formic acid, acetic acid, methane, or ethane was identified. At later photolysis times formic acid and acetic acid decrease in concentration, $^{13}CO_2$ and ^{13}CO concentrations remain constant, and CO_2 and CO concentrations continue to increase. This implies that the lactic acid supply has been depleted and remaining increases in product concentrations are due to acetic acid and formic acid photolysis[34-35].

Results from the gas-phase ^{13}C-tagged lactic acid photolysis offer important information regarding the origin of each of the products. Notably, only CO_2 and CO possess the ^{13}C, indicating C_1-C_2 bond cleavage as the initial step. In the case of C_1-C_2 bond cleavage, the resultant $HO^{13}CO$ radical would decompose to form $^{13}CO_2$ or ^{13}CO[11b]. It is also possible that $HO^{13}CO$ takes part in a bimolecular reaction before decomposition. In the case of reaction with small molecules, HOCO typically acts as a

hydrogen donor and produces CO_2[11b]. As we cannot detect short lived radicals using our techniques, we cannot distinguish between these two pathways, but there is good agreement between our identified products and the known products of HOCO chemistry[11b].

Due to the lack of ^{13}C tags, acetic acid, formic acid, methane, and ethane must all predominantly form from the alpha/secondary and beta/terminal lactic acid carbons. Additionally, untagged CO_2 and CO indicates secondary chemistry, likely due to formic acid and acetic acid photolysis which has been studied previously[13b, 34-35]. It is also worth noting the significant production of untagged CO throughout the experiment. While CO is a known product of formic acid photolysis, the prevalence of untagged CO as the dominant product compared to tagged products indicates secondary chemistry occurs rapidly and readily on both secondary and terminal carbons.

Aqueous Phase Photolysis

Aqueous lactic acid photolysis experiments were also performed as described in Methods. 100 mM solutions were placed in the photolysis cell and the cell was evacuated to remove dissolved gasses, including O_2, from the solution. Gas-phase species were monitored *in situ* by FTIR, and aqueous species were identified by ^1H NMR before and after reaction. FTIR spectra showed CO_2, CO, methane, and ethane formation in the gas phase above the solution. Once products were visually identified, the CEAM ANIR program was used to determine concentrations across spectra and product formation over time is shown in Figure 8. CO_2 is the main gas-phase product with CO, methane, and ethane as minor products.

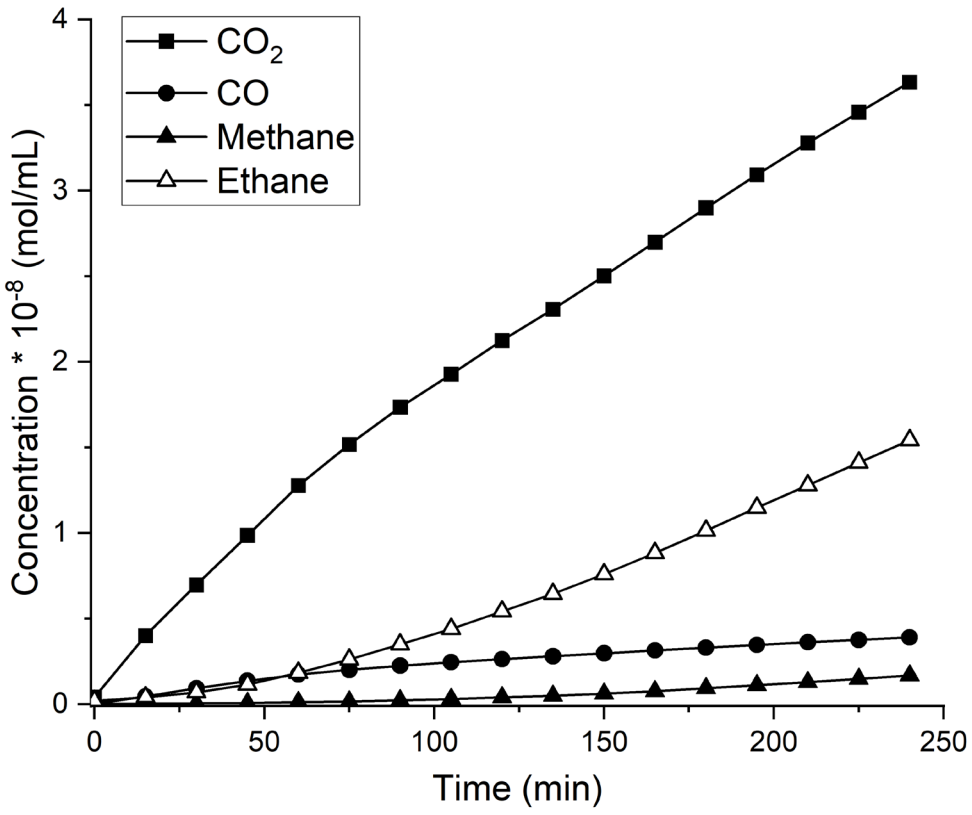

Figure 8: Gas-phase product formation over time recorded during aqueous lactic acid photolysis. CO_2 is the main gas-phase product produced by aqueous lactic acid photolysis with CO, ethane, and methane being minor products.

Aqueous products were identified in ^{1}H NMR spectra and include ethanol, formic acid, 2,3-butanediol, and isopropyl alcohol. A representative ^{1}H NMR spectrum with peak assignments for each product and the corresponding molecular structures is shown in Figure 9.

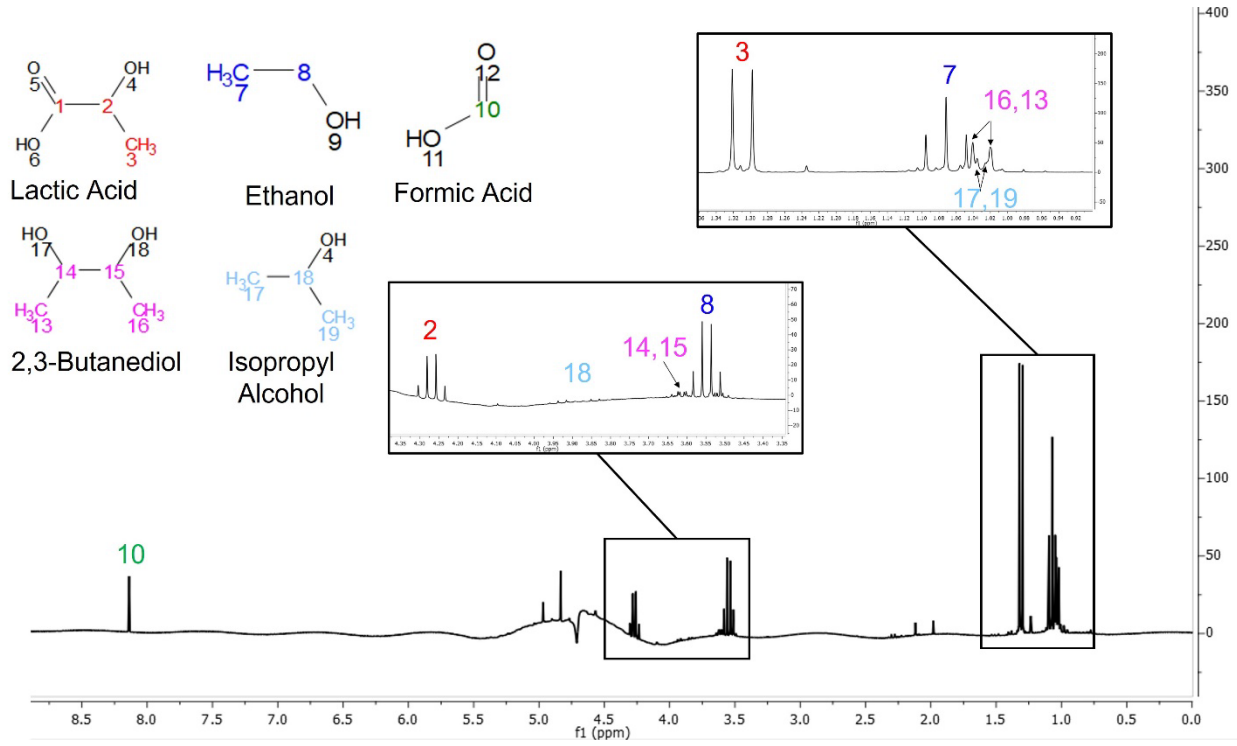

Figure 9: Representative ^{1}H NMR spectrum for products obtained from photolysis of lactic acid in H_2O. Insets are included for clarity. Samples were prepared as described in Methods. The water peak at 4.71 ppm has been suppressed using MestReNova resulting in the uneven baseline. Product structures are shown in the top left and peaks are attributed to the protons in lactic acid (red), ethanol (blue), formic acid (green), 2,3-butanediol (magenta), and isopropyl alcohol (light blue).

Ethanol, accounting for approximately half of the product concentration, is the main product of aqueous lactic acid photolysis which is consistent with previous studies performed under anoxic conditions[14a]. Formic acid and 2,3-butanediol each account for ~20% of the product concentration and isopropyl alcohol accounts for ~10% of the product concentration. Formic acid and 2,3-butanediol have been identified as minor products in previous studies[2a, 14b], but to the best of our knowledge, isopropyl alcohol has not been noted before.

Aqueous lactic acid photolysis was also studied using ^{13}C-tagged lactic acid, with the ^{13}C located at the primary, carboxyl, carbon, structure shown in SI. Experiments were performed as described in Methods and above for untagged lactic acid photolysis. FTIR spectra showed $^{13}CO_2$, CO_2, ^{13}CO, CO, methane, and ethane formation. No ^{13}C was found in the produced methane or ethane. Once products were visually identified, the

CEAM ANIR program was used to determine concentrations across spectra and example product formation over time is shown in Figure 10.

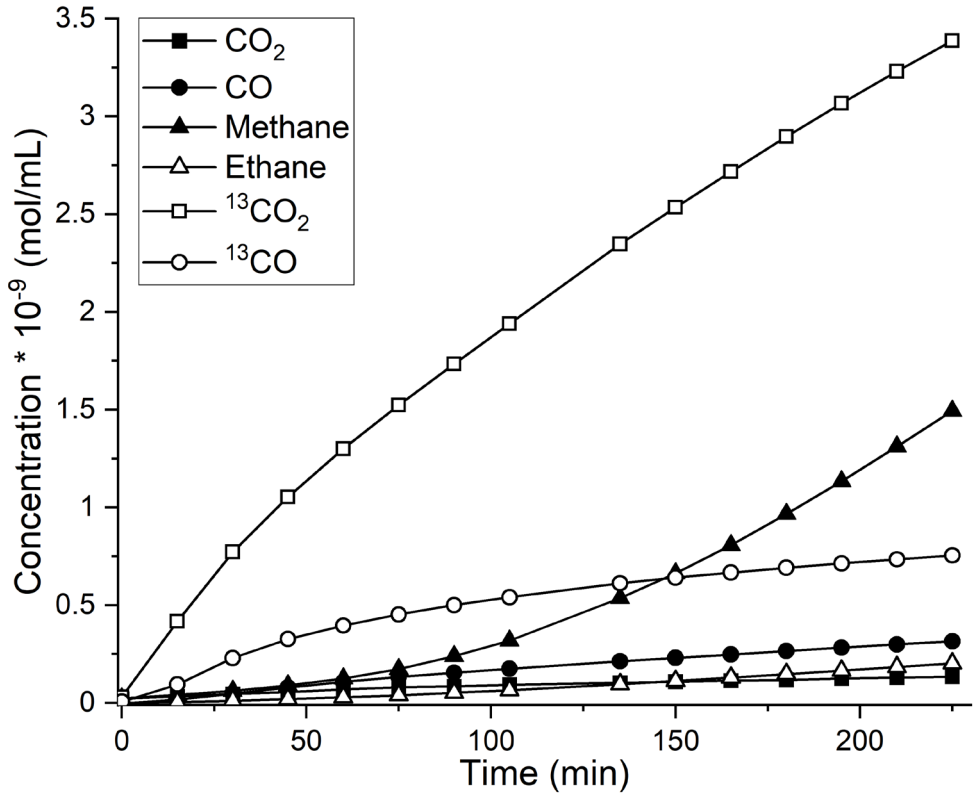

Figure 10: Gas-phase product formation over time measured during aqueous ^{13}C-tagged lactic acid photolysis. $^{13}CO_2$ is the main gas-phase product produced by aqueous lactic acid photolysis with CO_2, ^{13}CO, CO, ethane, and methane being additional products.

The ^{1}H NMR spectra obtained from aqueous ^{13}C-tagged lactic acid photolysis were also examined for ^{13}C-tagged products. As with untagged lactic acid, the aqueous products include ethanol, formic acid, 2,3-butanediol, and isopropyl alcohol. A representative ^{1}H NMR spectrum showing the peak assignments for each product of aqueous ^{13}C-tagged lactic acid photolysis and the corresponding molecular structures are shown in Figure 11.

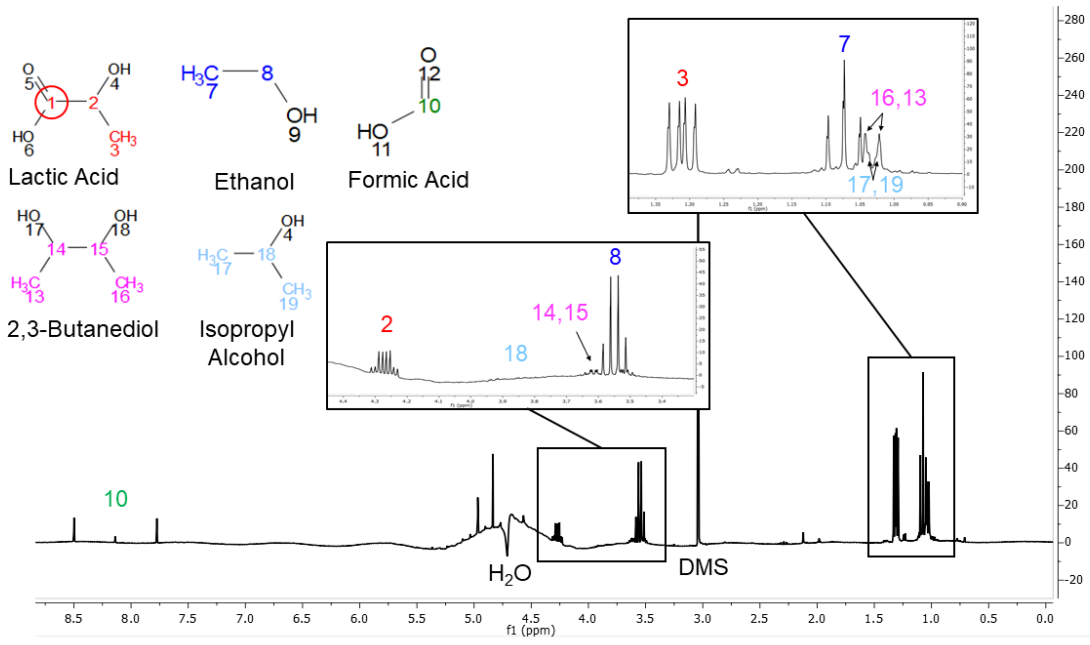

Figure 11: Representative ^{1}H NMR spectrum for products obtained from photolysis of ^{13}C-tagged lactic acid in H_2O. Insets are provided for clarity. Samples were prepared as described in Methods and the water peak at 4.71 ppm has been suppressed using MestReNova which results in the uneven baseline. Structures are shown in the top left and the location of the ^{13}C in lactic acid is circled in red. Peaks are attributed to the protons in lactic acid (red), ethanol (blue), formic acid (green), 2,3-butanediol (magenta), and isopropyl alcohol (light blue). Both ^{13}C-tagged and untagged formic acid are present as indicated by peak 10. No other product molecules show evidence of ^{13}C.

Interestingly, most of the produced formic acid is tagged with ^{13}C as indicated by the large satellite peaks surrounding feature number 10 in Figure 11. The presence of this isotopic carbon means that formic acid production in the aqueous phase predominantly occurs from the carboxylic group of lactic acid, a mechanistic path not accessible in the gas-phase photochemical experiments. We again assign C_1-C_2 bond cleavage, which creates a HO^{13}CO radical, as the initial photolysis step for aqueous lactic acid photolysis. In addition to forming $^{13}CO_2$ and ^{13}CO as seen in gas-phase photolysis, aqueous HO^{13}CO forms ^{13}C-tagged formic acid, likely due to hydrogen abstraction, either from lactic acid or its photolysis products.

Some formic acid is also produced from the alpha/secondary and/or beta/terminal lactic acid carbons, but this pathway appears significantly diminished as compared to

gas-phase photolysis. No ^{13}C was identified in ethanol, 2,3-butanediol, or isopropyl alcohol indicating they are produced solely from the alpha/secondary and/or beta/terminal lactic acid carbons.

Finally, aqueous lactic acid photolysis was studied using untagged lactic acid in D_2O. The resultant FTIR spectra identified the same products: CO_2, CO, methane, and ethane, see SI for concentration trends. The methane and ethane were not deuterated indicating that there is no hydrogen abstraction from the solvent during their production. Aqueous products again include ethanol, formic acid, 2,3-butanediol, and isopropyl alcohol. A representative ^1H spectrum showing the peak assignments for each product and the corresponding molecular structures are shown in Figure 12.

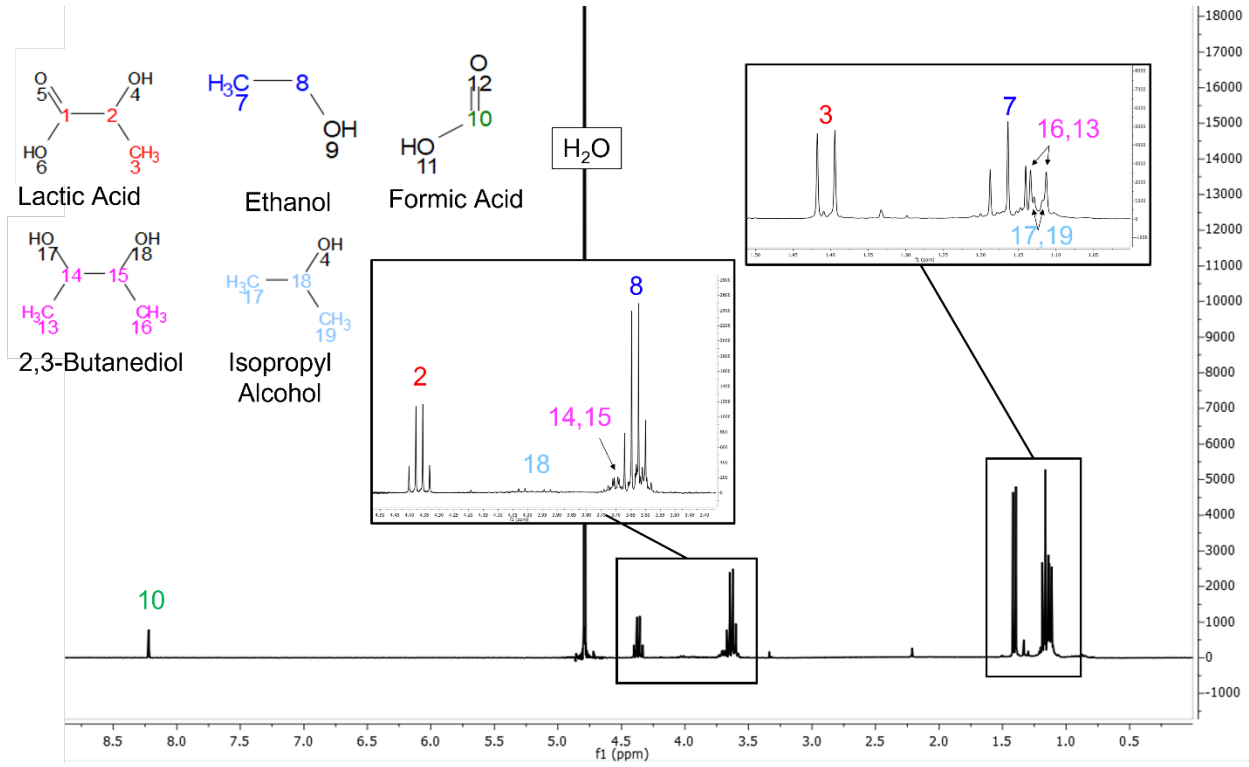

Figure 12: Representative ^1H NMR for products obtained from photolysis of lactic acid in D_2O. Structures are shown in the top left and peaks are attributed to the protons in lactic acid (red), ethanol (blue), formic acid (green), 2,3-butanediol (magenta), and isopropyl alcohol (light blue). No products show evidence of neighboring deuterated carbons.

We would expect that deuterated products, specifically deuterium attached directly to a carbon, would appear as a change in the multiplet structure for adjacent

protons. For example, if ethanol was deuterated at the central carbon forming CH_3CHDOD, the triplet corresponding to CH_3 protons would be reduced to a doublet. It is worth noting that although all alcohol groups are expected to exchange with the solvent, alcohol protons are not detected under our scan parameters and OH and OD can therefore not be distinguished in these NMR spectra. Additionally, deuterated formic acid (DCOOD) will not be detectable under our conditions due to the absence of any adjacent protons. However, the detection of formic acid (peak 10 in Figure 12) indicates that a significant portion of all produced formic acid has a hydrogen attached to the carbon (HCOOD). Despite the limitations, we can safely infer that none of the lactic acid photolysis intermediates or products abstract hydrogen from the solvent. Furthermore, due to the deuteration of alcohol groups in D_2O, we can also rule out abstraction from alcohol groups and specify that radicals must abstract hydrogen from hydrogenated carbons on lactic acid or its derivatives.

Photolysis Mechanisms

Three potential lactic acid photodecomposition mechanisms were investigated computationally by calculating CBS-QB3 bond dissociation enthalpies (BDEs). The three mechanisms and the associated BDEs are shown in Scheme 1. We note that the BDEs reported here are for the SsC conformer, but BDEs for the other conformers vary only by the overall enthalpy difference, see SI for details. The bond dissociation mechanisms investigated here include C_1-C_2 bond scission (1a), C_2-OH bond scission resulting in removal of the α-hydroxyl group (1b), and C_2-C_3 bond scission resulting removal of the methyl group (1c).

Scheme 1. Initial Photodecomposition Mechanisms for Lactic Acid Following Excitation at 5.0 to 5.6 eV and Associated Bond Dissociation Enthalpies.

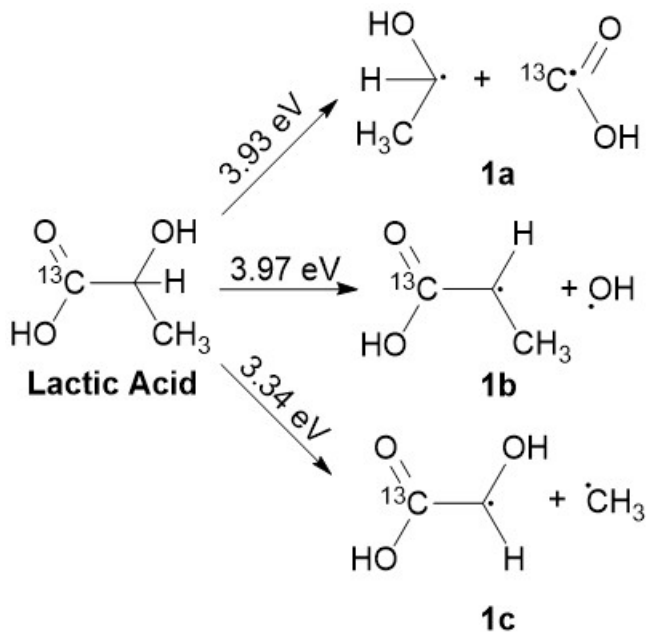

Methyl dissociation (1c) has the lowest BDE, but all three pathways are energetically accessible given the absorption of photons with energies between 5.0 and 5.6 eV (λ = 220 – 250 nm). Previously, α-hydroxyl group removal (1b) has been investigated by Thøgersen et al. using a time resolved experiment on aqueous lactate films using a UV pump (λ=200 nm) and IR probe.[12a] They proposed that α-hydroxyl group removal would be energetically competitive with C_1-C_2 bond cleavage in aqueous lactate (deprotonated lactic acid), but they mainly observed products consistent with C_1-C_2 bond cleavage. It is also worth noting that many of the expected final products from mechanisms with α-hydroxyl or methyl group removal as the initial step are either not detectable using our experimental methods or cannot be distinguished from those expected from mechanisms with C_1-C_2 scission as the initial step. This is discussed later.

The S_1 excited states were probed using DFT to elucidate the possible dissociation processes. We calculated adiabatic electronic excitation energies by optimizing the geometry of the S_1 state and the results are 4.98 eV, 4.78 eV, 4.82 eV, 4.77 eV, 4.83 eV, 4.90 eV and 4.72 eV for the SsC, GskC, G'sk'C, AaT, AsC, SsT, and AaC conformers, respectively. The peak overlap between the actinic flux of our lamp and absorption by lactic acid occurs at 230 nm or ~5.4 eV in our experiments, see Figure 5. At this

wavelength, the photon is depositing approximately 0.4 to 0.7 eV of excess energy in the excited molecule, allowing for ergodicity in the S_1 state which may lead to dissociation. Excited state geometries provide further clues as to which part of the molecule is initially activated. The carboxylic acid group, specifically the carbonyl bond geometry, is significantly altered in the excited state. For all conformers, the carbonyl bond elongates by ~0.1 Å and the C_1-OH bond elongates by ~0.04 Å, while other bond lengths are mostly unchanged, indicating that the carboxylic acid group acts as the chromophore.

It is also interesting that the VEE of the first singlet transition in the SsC and SsT conformers is significantly higher energy than the VEEs in the other investigated conformers. The SsC and SsT conformers are the only conformers with an internal hydrogen bond involving the C_1=O group as an acceptor and we see that the internal hydrogen bond in the SsC conformer is broken in the excited state geometry as shown in Figure 13. Accordingly, changes in the electronic configuration of the C_1=O group upon excitation likely explain the higher VEEs. To clarify this point, we compare the SsC and AsC conformers as they differ only by a 180° rotation of the O-H donor, removing the internal hydrogen bond going from the SsC to the AsC conformer, see Figure 1. Between the SsC and AsC conformers, the calculated gas-phase VEE for the S_0 to S_1 excitation for SsC is 0.25 eV higher and the ground state electronic energy of the SsC conformer is 0.21 eV lower. The difference between ground state electronic energies is likely due to the internal hydrogen bond which stabilizes the SsC conformer. Thus, electronic excitations in the SsC and SsT conformers must provide enough extra energy to break the internal hydrogen bond making the total VEE higher than that of other conformers.

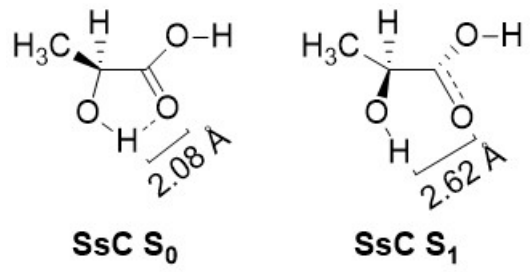

Figure 13. Relaxed geometries of the lactic acid conformer SsC in the ground state (S_0, left) and first excited singlet state (S_1, right) calculated at the ωB97X-D/aug-cc-pVTZ level. The excited state optimization was done with unrestricted Kohn-Sham. The intramolecular hydrogen bond present in the ground state (denoted by the dotted line) is absent in the excited state.

We can now look to experimental results that show final photolysis products to infer the primary dissociation mechanism. The main products from gas-phase lactic acid photolysis were CO and CO_2. Photolysis of gas-phase ^{13}C-tagged lactic acid demonstrated that a significant portion of the formed CO_2 and CO originate from the carboxyl carbon as depicted in Scheme 2. No other products of gas-phase photolysis originating from the carboxyl carbon were identified.

Scheme 2. Proposed Initial Lactic Acid Photolysis Steps

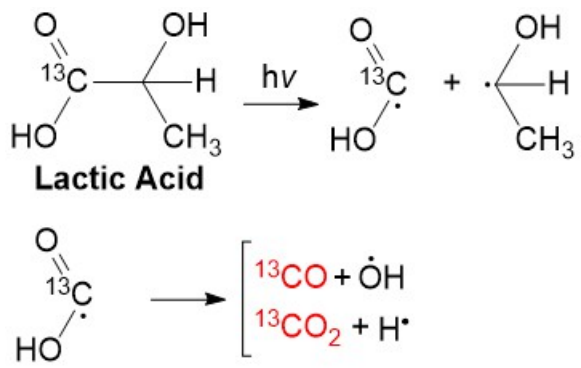

This exclusive and rapid formation of $^{13}CO_2$ and ^{13}CO from the carboxyl carbon implies C_1-C_2 bond scission as the primary step in lactic acid photolysis. Such C_1-C_2 bond breakage would result in a HOCO radical group which is well studied and known to decompose to form CO and CO_2 with CO/HO· being the dominant photochemical decomposition product[11b].

Acetic acid, formic acid, methane, and ethane were also identified as minor products from gas-phase lactic acid photolysis. None of these contained isotopic carbon upon photolysis of ^{13}C -tagged lactic acid and therefore must be produced from the alpha and beta/terminal carbons. Assuming C_1-C_2 bond breakage as the primary photolysis step, the alpha and beta/terminal carbons form a CH_3CHOH radical which may undergo complex, multistep, radical chemistry. One potential fate involving acetaldehyde as an intermediate is shown in Scheme 3.

Scheme 3. Proposed Mechanism for Methane and Ethane Formation During Gas-phase Lactic Acid Photolysis[a]

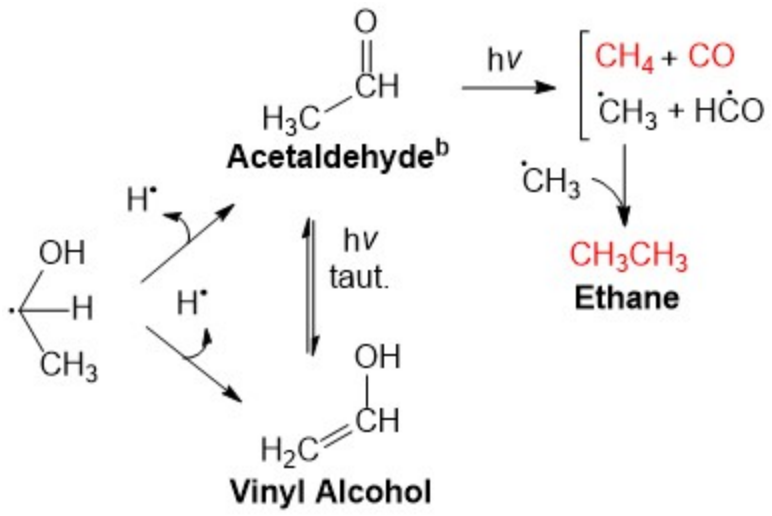

[a]Products observed by gas-phase FTIR are highlighted in red
[b]Acetaldehyde photochemistry and phototautomerization has been previously studied[37]

If the CH_3CHOH radical loses a hydrogen from the alcohol group, it will form acetaldehyde and if it loses a hydrogen from the methyl group it will form vinyl alcohol. Acetaldehyde and vinyl alcohol are tautomers and will strive towards thermal equilibrium, but studies have shown irradiation can also induce phototautomerization of acetaldehyde to form vinyl alcohol. Although we do not detect acetaldehyde or vinyl alcohol, it is not surprising as the acetaldehyde tautomer is photoactive with an estimated photolysis rate up to 7 times higher than that of acetic acid and formic acid. This estimate was calculated by assuming a quantum yield of 1[34-35] for all species and integrating over the absorption cross sections[12b] multiplied by the actinic flux in our experiments. Additionally, key acetaldehyde vibrational features overlap with other products. This difficulty in detection and expected rapid photolysis would likely make acetaldehyde difficult to discern in our FTIR spectra. We do, however, detect one of its known products, methane, which is unique from the products of all other proposed mechanistic pathways following C_1-C_2 bond scission. Additionally, acetaldehyde photolysis is known to produce methyl radicals which could form ethane as we suggest in Scheme 3.

We note that methyl radicals could also be formed directly by C_2-C_3 bond scission in lactic acid as shown in Scheme 1, pathway 1c. If this mechanism were to occur, the remaining HCOHCOOH radical would likely decompose or form glycolic acid or gloxylic acid which are both photoactive[38]. The expected products of C_2-C_3 bond scission cannot be distinguished from those already identified. However, given the experimental evidence supporting the C_1-C_2 bond scission mechanism presented in Scheme 2, it appears that

C_1-C_2 scission is the dominant initial pathway. This leads us to believe that C_2-C_3 bond scission is at most a minor pathway and C_1-C_2 bond scission, by way of acetaldehyde, is the main, if not only, source of methyl radicals.

Formic acid and acetic acid are also each photochemically active and known to produce CO, CO_2, and an assortment of radicals including hydroxyl and hydrogen radicals[34-35]. It is difficult to discern the mechanistic pathways leading to formic acid and acetic acid, but they likely involve radical chemistry. Regardless, acetic acid and formic acid are both clearly identifiable as photolysis products and are likely large sources of secondary chemistry. Specifically, secondary photolysis of acetic acid and formic acid is likely a large contributor to the overall CO and CO_2 yield as we see a significant amount of non-tagged CO and CO_2 that continues to increase even as the lactic acid availability appears to plateau.

Aqueous lactic acid photolysis experiments also support C_1-C_2 bond scission as the initial photochemical step. The dominant gas-phase products formed during aqueous lactic acid photolysis are CO_2 and CO, as was the case for gas-phase lactic acid photolysis. The dominant condensed phase product from aqueous lactic acid photolysis was ethanol, which is consistent with previous studies performed under anoxic conditions[2a, 14]. We also observe 2,3-butanediol, isopropyl alcohol, and formic acid as products in the condensed phase. Minor gas-phase products produced during aqueous photolysis were methane and ethane as was noted for gas-phase photolysis. Scheme 4 presents a proposed mechanism for aqueous lactic acid photolysis with gas-phase products identified by FTIR shown in red and condensed phase products identified by ^{1}H NMR shown in blue.

Scheme 4: Proposed Mechanism for Photolysis of Aqueous Lactic Acid[a]

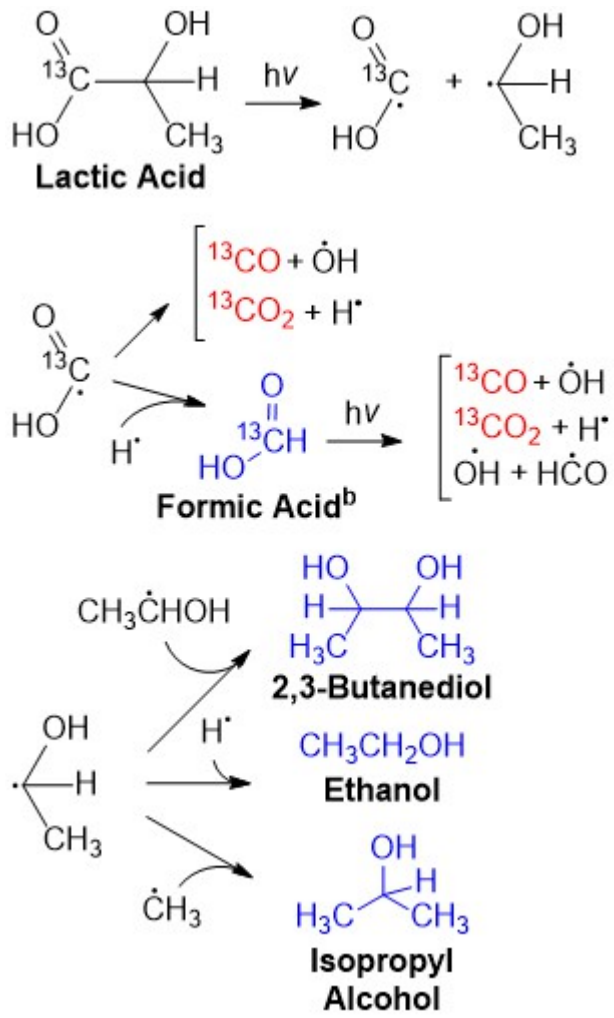

[a]Products observed by gas-phase FTIR are highlighted in red, and products observed by ^{1}H NMR are highlighted in blue

[b]Formic acid photochemistry has been previously studied[35]

As with gas-phase photolysis, we propose that the initial cleavage mechanism of excited lactic acid in water involves decomposition into a HOCO and CH_3CHOH radical as shown in Scheme 4. This is strongly supported by ^{13}CO and $^{13}CO_2$ production, which likely requires $HO^{13}CO$ formation and subsequent decomposition, and 2,3-butanediol production, which likely requires two CH_3CHOH radicals to recombine.

After this initial step, however, the subsequent chemistry in the aqueous phase differs from that of the gas phase. First, the product 2,3-butanediol demonstrates that radical lifetimes in the aqueous environment are long enough to support diffusion and subsequent recombination via bimolecular reaction. Additionally, aqueous ^{13}C-tagged lactic acid photolysis demonstrated the carboxyl carbon can form formic acid, as well as the $^{13}CO_2$ and ^{13}CO identified in gas-phase photolysis. All remaining products (ethanol, 2,3-butanediol, isopropyl alcohol, methane, ethane, and a small portion of formic acid) were not tagged indicating they are produced from the alpha/secondary and/or beta/terminal lactic acid carbons.

Photochemistry of lactic acid in D_2O indicates that the solvent does not act as a reactant in this chemistry and radicals, such as the precursors to ethanol and formic acid, must abstract a hydrogen from hydrogenated carbons in lactic acid or its derivatives. In the case of ethanol, this also rules out a 1,2-sigmatropic shift from the alcohol group to the radical carbon center as this would form CH_3CHDOD. Instead, we can speculate that the longevity of radicals as indicated by 2,3-butanediol also allows for hydrogen abstraction from other solute molecules.

The mechanistic pathway suggested for the gas phase wherein the CH_3CHOH radical forms acetaldehyde is likely also applicable in the aqueous phase as shown in Scheme 5. Again, we do not detect acetaldehyde, but it likely photolyzes rapidly to produce methane, which we detect by FTIR, and methyl radicals.

Scheme 5: Proposed Mechanistic Pathway Producing Isopropyl Alcohol, Methane, and Ethane During Aqueous Lactic Acid Photolysis[a,b]

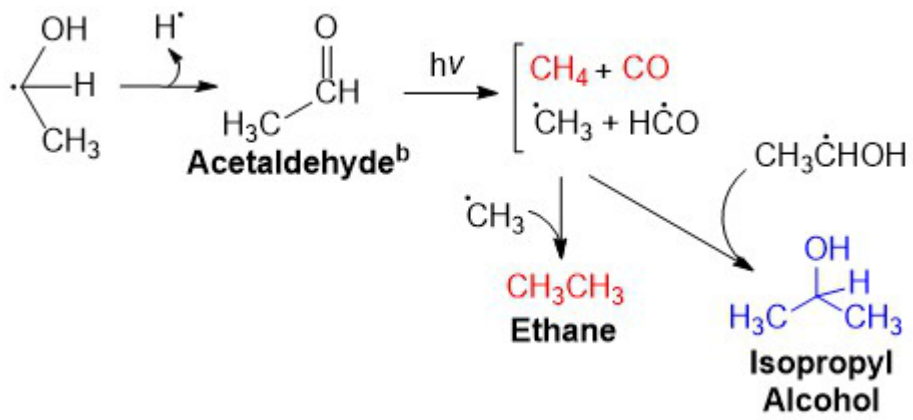

[a]Products observed by gas-phase FTIR are highlighted in red, and products observed by ^1H NMR are highlighted in blue

[b]Acetaldehyde[37a] photochemistry has been previously studied

We propose that methyl radical formation via acetaldehyde photolysis may explain ethane and isopropyl alcohol production. The longevity of photochemically formed aqueous radicals, as indicated by 2,3-butanediol, suggests methyl radicals could combine with a CH_3CHOH radical to form isopropyl alcohol or another methyl radical to form ethane. Again, we note that direct C_2-C_3 bond scission as the initial photolysis step could also provide methyl radicals, but we posit that this would be at most a minor pathway. Regardless of exact mechanism, this is the first time isopropyl alcohol has been identified as a lactic acid photolysis product. The photolysis lamp used in this study is more powerful than those used in previous studies which likely increased secondary photochemistry and may have provided the extra methyl radicals necessary to form isopropyl alcohol.

In summary, we have presented evidence using isotopic labelling that lactic acid photodecomposes predominantly via C_1-C_2 bond scission, both in gas and aqueous phases. This is consistent with a recent study concerning the high energy photolysis of aqueous lactic acid which proposed a partial mechanism including pathways to CO_2, ethanol, formic acid, and 2,3-butanediol.[2a] We expand upon this proposed mechanism, largely through isotopic labeling of the carboxylic acid group which allowed us to infer almost exclusive C_1-C_2 bond cleavage following lactic acid excitation. This bond selectivity is initially surprising as the energy deposited in the molecule through S_0 to S_1 excitation exceeds the calculated BDEs of C_1-C_2, C_2-OH, and C_2-C_3 bonds, but may be supported by DFT calculations which suggest that the carboxylic acid group acts as the chromophore.

We also note that our techniques can only determine mechanistic information through final product identification, which for aqueous products may be analyzed hours after photolysis has completed. In some cases, this makes detailed mechanisms challenging to decipher, namely the formation of acetic acid and formic acid in the gas phase and the small amount of formic acid formed from the alpha/secondary and/or beta/terminal carbons in the aqueous phase. Regardless, using D_2O and isotopically labelled lactic acid, we tracked the fate of the carboxylic acid carbon and suggested reasonable mechanistic pathways consistent with our data.

It is perhaps worth briefly discussing the potential products should lactic acid decompose by one of the alternate paths: C_2-OH bond scission or C_2-C_3 bond scission. In the first case, the resultant carbon radical would likely either lose or gain a hydrogen forming either acrylic acid or propionic acid. In the second case, as described previously, the methyl radical could participate in secondary radical chemistry while the remaining

carbon radical would likely either lose or gain a hydrogen to form either glyoxylic acid or glycolic acid. Each of these molecules are themselves photoactive under our experimental conditions with most of the known products being the same as the end products we attribute to C_1-C_2 bond scission. Both FTIR spectra (for all photolysis experiments) and NMR spectra (for aqueous phase photolysis experiments) were examined for any signals that could be uniquely attributed to these alternate pathways and none were identified. Although we cannot definitively rule out C_2-OH or C_2-C_3 bond scission as an initial step, the literature[12a, 13] and the results in this work strongly suggest C_1-C_2 scission is the initial lactic acid photolysis step.

We also demonstrate that lactic acid photolysis is phase dependent with changes in both conformer ratios and accessible mechanisms. Using computation, we have shown that the S_0 to S_1 transition in the SsC and SsT conformers is blue shifted relative to the same transition in the other five identified conformers. This blue shift is explained by the extra energy require to break the internal hydrogen bond during excitation of the SsC and SsT conformers. This finding is significant for environments, such as the experiments presented here, where available radiation has a small overlap with lactic acid absorption, favoring photolysis of conformers with lower energy transitions. Depending on environmental conditions, specific conformers may contribute to photochemistry more or less than what their relative abundance would suggest.

Phase also affects final products, pointing to mechanistic differences. Gas-phase and aqueous photolysis share the major products of CO_2 and CO, but gas-phase photolysis otherwise mainly leads to formic acid (1 carbon) and acetic acid (2 carbons) while aqueous photolysis supports secondary mechanistic pathways that can lead to products with more carbons (2,3-butanediol: 4C, isopropyl alcohol: 3Cs, ethanol: 2Cs, and formic acid: 1C). It is also interesting to note that the formation of a single 2,3-butanediol molecule requires two lactic acid molecules; thus, approximately equal amounts of lactic acid end up as 2,3-butanediol and ethanol. Product variations in the number of carbons may be significant to both abiotic chemistry and biomass valorization.

Conclusions

We studied the photolysis of lactic acid after excitation of S_0 to S_1 with high energy radiation (E = 5.0 to 5.6 eV; λ = 220 to 250 nm) in both gas and aqueous phases. We show, using computation, that the peak absorption wavelength is conformer specific, meaning the contribution of each conformer to the overall photochemical process may be dependent on more than just the relative populations. We determine by a set of

experiments, and with computational support, that lactic acid primarily decarboxylates upon photochemical excitation. This work also establishes the phase differences for lactic acid photolysis as gas-phase photolysis, to the best of our knowledge, has not been previously studied.

Lactic acid photolysis could be useful for abiotic processing, whether for the formation of life, biomass valorization, or organic synthesis. Here we show three ways lactic acid photolysis could impact abiotic chemistry. First, we demonstrate that lactic acid photolysis induces a change in the oxidation state of carbon in the absence of free oxygen, and second, we confirm that aqueous lactic acid photolysis can form products with more carbons than the starting material, representing abiotic chemical processes which increase the system's molecular complexity. Last, in the case of 2,3-butanediol as compared to ethanol, understanding that both represent an equal amount of photolyzed lactic acid can help guide missions in the detection of lactic acid or its derivatives. Ethanol and 2,3-butanediol are also both functional molecules of interest for biomass valorization and we provide new mechanistic information regarding their production. Specifically, we show that the solvent does not act as a reactant in the process of forming such molecules; this knowledge can assist in the design of future processing methodologies and catalysts. Lactic acid, a multifunctional molecule found on modern Earth and in meteorites, has diverse, phase-dependent photochemistry. Understanding this photochemistry is important for predicting its behavior in environments subject to high energy radiation and for designing organic synthesis/biomass valorization processes that can capitalize on the multifunctionality of lactic acid.

Acknowledgements

This work was funded by the U. S. Army Research Office, grant #ARO W911NF1710115, and the National Science Foundation, grant #CHE 1611107. A.M.D. acknowledges funding from the National Science Foundation Graduate Research Fellowship, grant #DGE 1650115. B.N.F acknowledges funding from the Independent Research Fund, Denmark, grant #9056-00005B. We thank Barney Ellison for multiple useful and interesting discussions regarding mechanisms. We also thank Bimala Lama for the helpful discussions regarding NMR sample preparation and analysis and the University of Colorado at Boulder Nuclear Magnetic Resonance Spectroscopy Facility for the use of their instruments.

References

[1] a) J. G. Forsythe, S. S. Yu, I. Mamajanov, M. A. Grover, R. Krishnamurthy, F. M. Fernandez, N. V. Hud, *Angew. Chem. Int. Ed.* **2015**, *54*, 9871-9875; b) T. Z. Jia, K. Chandru, Y. Hongo, R. Afrin, T. Usui, K. Myojo, H. J. Cleaves, *Proc. Natl. Acad. Sci. U. S. A.* **2019**, *116*, 15830-15835; c) J. K. Lee, D. Samanta, H. G. Nam, R. N. Zare, *J. Am. Chem. Soc.* **2019**, *141*, 10585-10589; d) A. M. Deal, R. J. Rapf, V. Vaida, *J. Phys. Chem. A* **2021**, *125*, 4929-4942; e) K. J. Kappes, A. M. Deal, M. F. Jespersen, S. L. Blair, J. F. Doussin, M. Cazaunau, E. Pangui, B. N. Hopper, M. S. Johnson, V. Vaida, *J. Phys. Chem. A* **2021**, *125*, 1036-1049.

[2] a) K. Liu, A. Litke, Y. Su, B. G. van Campenhout, E. A. Pidko, E. J. Hensen, *Chem. Commun. (Camb.)* **2016**, *52*, 11634-11637; b) D. Rodríguez-Padrón, A. R. Puente-Santiago, A. M. Balu, M. J. Muñoz-Batista, R. Luque, *ChemCatChem* **2018**, *11*, 18-38; c) Y. Fan, C. Zhou, X. Zhu, *Catalysis Reviews* **2009**, *51*, 293-324; d) E. S. Lipinsky, R. G. Sinclair, *Chem. Eng. Prog.* **1986**, *82*, 26-32; e) L. S. Sharninghausen, J. Campos, M. G. Manas, R. H. Crabtree, *Nature Comm.* **2014**, *5*, 1-9; f) R. F. Lobo, *ChemSusChem* **2010**, *3*, 1237-1240; g) A. V. Puga, *Coord. Chem. Rev.* **2016**, *315*, 1-66.

[3] E. T. Peltzer, J. L. Bada, *Nature* **1978**, *272*, 443-444.

[4] a) R. J. Rapf, R. J. Perkins, B. K. Carpenter, V. Vaida, *J. Phys. Chem. A* **2017**, *121*, 4272-4282; b) E. C. Griffith, B. K. Carpenter, R. K. Shoemaker, V. Vaida, *Proc. Natl. Acad. Sci. U. S. A.* **2013**, *110*, 11714-11719.

[5] a) S. L. Miller, H. C. Urey, *Science* **1959**, *130*, 245-251; b) R. J. Rapf, V. Vaida, *Phys. Chem. Chem. Phys.* **2016**, *18*, 20067-20084; c) E. C. Griffith, A. F. Tuck, V. Vaida, *Acc. Chem. Res.* **2012**, *45*, 2106-2113.

[6] a) T. B. Nguyen, J. Laskin, A. Laskin, S. A. Nizkorodov, *Environ. Sci. Technol.* **2011**, *45*, 6908-6918; b) H. Li, O. Kupiainen-Maatta, H. J. Zhang, X. H. Zhang, M. F. Ge, *Atmos. Environ.* **2017**, *166*, 479-487; c) D. Pagonis, D. J. Price, L. B. Algrim, D. A. Day, A. V. Handschy, H. Stark, S. L. Miller, J. de Gouw, J. L. Jimenez, P. J. Ziemann, *Environ. Sci. Technol.* **2019**, *53*, 4794-4802; d) R. S. Gordon, R. H. Thompson, J. Muenzer, D. Thrasher, *J. Appl. Physiol.* **1971**, *31*, 713-&.

[7] M. Gavahian, P. E. S. Munekata, I. Eş, J. M. Lorenzo, A. Mousavi Khaneghah, F. J. Barba, *Green Chem.* **2019**, *21*, 1171-1185.

[8] S. Maina, A. A. Prabhu, N. Vivek, A. Vlysidis, A. Koutinas, V. Kumar, *Biotechnol. Adv.* **2021**, 107783.

[9] a) S. Ranjan, D. D. Sasselov, *Astrobiology* **2016**, *16*, 68-88; b) J. F. Kasting, *Geological Society of America Special Papers* **2014**, *504*, 19-28.

[10] a) A. E. Reed Harris, A. Pajunoja, M. Cazaunau, A. Gratien, E. Pangui, A. Monod, E. C. Griffith, A. Virtanen, J. F. Doussin, V. Vaida, *J. Phys. Chem. A*

2017, *121*, 3327-3339; b) S. L. Blair, A. E. R. Harris, B. N. Frandsen, H. G. Kjaergaard, E. Pangui, M. Cazaunau, J. F. Doussin, V. Vaida, *J. Phys. Chem. A* **2020**, *124*, 1240-1252.
[11] a) M. R. Alves, Y. Fang, K. J. Wall, V. Vaida, V. H. Grassian, *J. Phys. Chem. A* **2019**, *123*, 7661-7671; b) J. S. Francisco, J. T. Muckerman, H. G. Yu, *Acc. Chem. Res.* **2010**, *43*, 1519-1526.
[12] a) J. Thogersen, V. Vaida, M. Bregnhoj, T. Weidner, F. Jensen, *Phys. Chem. Chem. Phys.* **2021**, *23*, 4555-4568; b) H. Keller-Rudek, G. K. Moortgat, R. Sander, R. Sorensen, *Earth Syst. Sci. Data* **2013**, *5*, 365-373.
[13] a) J. Thogersen, T. Weidner, F. Jensen, *Phys. Chem. Chem. Phys.* **2021**, *23*, 10040-10050; b) M. M. Madsen, F. Jensen, S. J. Knak Jensen, J. Thogersen, *Phys. Chem. Chem. Phys.* **2019**, *21*, 7358-7366.
[14] a) G. R. Burns, *J. Am. Chem. Soc.* **1929**, *51*, 3165-3171; b) G. R. Burns, *J. Am. Chem. Soc.* **1930**, *52*, 5272-5278.
[15] a) B. N. Frandsen, A. M. Deal, J. R. Lane, V. Vaida, *J. Phys. Chem. A* **2021**, *125*, 218-229; b) J. Sadlej, J. C. Dobrowolski, J. E. Rode, M. H. Jamroz, *Phys. Chem. Chem. Phys.* **2006**, *8*, 101-113; c) L. Pszczolkowski, E. Bialkowska-Jaworska, Z. Kisiel, *J. Mol. Spectrosc.* **2005**, *234*, 106-112; d) A. Borba, A. Gomez-Zavaglia, L. Lapinski, R. Fausto, *Phys. Chem. Chem. Phys.* **2004**, *6*, 2101-2108; e) C. D. Zeinalipour-Yazdi, C. R. A. Catlow, *Phys. Chem. Chem. Phys.* **2019**, *21*, 22331-22343; f) A. S. Perera, J. Cheramy, M. R. Poopari, Y. J. Xu, *Phys. Chem. Chem. Phys.* **2019**, *21*, 3574-3584; g) M. Pecul, A. Rizzo, J. Leszczynski, *J. Phys. Chem. A* **2002**, *106*, 11008-11016.
[16] A. E. Reed Harris, J. F. Doussin, B. K. Carpenter, V. Vaida, *J. Phys. Chem. A* **2016**, *120*, 10123-10133.
[17] L. S. Rothman, I. E. Gordon, A. Barbe, D. C. Benner, P. F. Bernath, M. Birk, V. Boudon, L. R. Brown, A. Campargue, J.-P. Champion, *J. Quant. Spectrosc. Radiat. Transfer* **2009**, *110*, 533-572.
[18] J. A. Montgomery, M. J. Frisch, J. W. Ochterski, G. A. Petersson, *J. Chem. Phys.* **1999**, *110*, 2822-2827.
[19] J. D. Chai, M. Head-Gordon, *J. Chem. Phys.* **2008**, *128*.
[20] T. H. Dunning, *J. Chem. Phys.* **1989**, *90*, 1007-1023.
[21] E. Runge, E. K. U. Gross, *Phys. Rev. Lett.* **1984**, *52*, 997-1000.
[22] J. Tomasi, B. Mennucci, R. Cammi, *Chem. Rev.* **2005**, *105*, 2999-3093.
[23] a) V. Barone, *J. Chem. Phys.* **2004**, *120*, 3059-3065; b) J. Bloino, V. Barone, *J. Chem. Phys.* **2012**, *136*; c) V. Barone, *J. Chem. Phys.* **2005**, *122*; d) J. Bloino, M. Biczysko, V. Barone, *J. Phys. Chem. A* **2015**, *119*, 11862-11874; e) R. L. Jacobsen, R. D. Johnson, K. K. Irikura, R. N. Kacker, *J. Chem. Theory Comput.* **2013**, *9*, 951-954.

[24] a) A. D. Becke, *J. Chem. Phys.* **1993**, *98*, 1372-1377; b) C. T. Lee, W. T. Yang, R. G. Parr, *Phys. Rev. B Condens. Matter Mater. Phys.* **1988**, *37*, 785-789.
[25] E. Papajak, J. J. Zheng, X. F. Xu, H. R. Leverentz, D. G. Truhlar, *J. Chem. Theory Comput.* **2011**, *7*, 3027-3034.
[26] a) H. Koch, H. J. A. Jensen, P. Jorgensen, T. Helgaker, *J. Chem. Phys.* **1990**, *93*, 3345-3350; b) J. F. Stanton, R. J. Bartlett, *J. Chem. Phys.* **1993**, *98*, 7029-7039.
[27] a) T. Clark, J. Chandrasekhar, G. W. Spitznagel, P. V. Schleyer, *J. Comput. Chem.* **1983**, *4*, 294-301; b) R. Krishnan, J. S. Binkley, R. Seeger, J. A. Pople, *J. Chem. Phys.* **1980**, *72*, 650-654.
[28] G. D. Purvis, R. J. Bartlett, *J. Chem. Phys.* **1982**, *76*, 1910-1918.
[29] a) A. D. Laurent, A. Blondel, D. Jacquemin, *Theor. Chem. Acc.* **2015**, *134*; b) M. Schreiber, M. R. Silva, S. P. A. Sauer, W. Thiel, *J. Chem. Phys.* **2008**, *128*; c) R. Izsak, *Wiley Interdiscip. Rev. Comput. Mol. Sci.* **2020**, *10*.
[30] M. J. Frisch, G. W. Trucks, H. B. Schlegel, G. E. Scuseria, M. A. Robb, J. R. Cheeseman, G. Scalmani, V. Barone, G. A. Petersson, H. Nakatsuji, X. Li, M. Caricato, A. V. Marenich, J. Bloino, B. G. Janesko, R. Gomperts, B. Mennucci, H. P. Hratchian, J. V. Ortiz, A. F. Izmaylov, J. L. Sonnenberg, Williams, F. Ding, F. Lipparini, F. Egidi, J. Goings, B. Peng, A. Petrone, T. Henderson, D. Ranasinghe, V. G. Zakrzewski, J. Gao, N. Rega, G. Zheng, W. Liang, M. Hada, M. Ehara, K. Toyota, R. Fukuda, J. Hasegawa, M. Ishida, T. Nakajima, Y. Honda, O. Kitao, H. Nakai, T. Vreven, K. Throssell, J. A. Montgomery Jr., J. E. Peralta, F. Ogliaro, M. J. Bearpark, J. J. Heyd, E. N. Brothers, K. N. Kudin, V. N. Staroverov, T. A. Keith, R. Kobayashi, J. Normand, K. Raghavachari, A. P. Rendell, J. C. Burant, S. S. Iyengar, J. Tomasi, M. Cossi, J. M. Millam, M. Klene, C. Adamo, R. Cammi, J. W. Ochterski, R. L. Martin, K. Morokuma, O. Farkas, J. B. Foresman, D. J. Fox, Wallingford, CT, **2016**.
[31] D. A. Matthews, L. Cheng, M. E. Harding, F. Lipparini, S. Stopkowicz, T. C. Jagau, P. G. Szalay, J. Gauss, J. F. Stanton, *J. Chem. Phys.* **2020**, *152*.
[32] a) B. P. Pritchard, D. Altarawy, B. Didier, T. D. Gibson, T. L. Windus, *J. Chem. Inf. Model.* **2019**, *59*, 4814-4820; b) K. L. Schuchardt, B. T. Didier, T. Elsethagen, L. S. Sun, V. Gurumoorthi, J. Chase, J. Li, T. L. Windus, *J. Chem. Inf. Model.* **2007**, *47*, 1045-1052.
[33] a) R. Crespo-Otero, M. Barbatti, *Theor. Chem. Acc.* **2012**, *131*; b) C. F. Fang, B. Oruganti, B. Durbeej, *J. Phys. Chem. A* **2014**, *118*, 4157-4171; c) S. Farahani, B. N. Frandsen, H. G. Kjaergaard, J. R. Lane, *J. Phys. Chem. A* **2019**, *123*, 6605-6617.
[34] W. H. Fang, R. Z. Liu, X. Zheng, D. L. Phillips, *J. Org. Chem.* **2002**, *67*, 8407-8415.

[35] H. M. Su, Y. He, F. N. Kong, W. H. Fang, R. Z. Liu, *J. Chem. Phys.* **2000**, *113*, 1891-1897.
[36] A. Loh, M. Wolff, *J. Quant. Spectrosc. Radiat. Transfer* **2017**, *203*, 517-521.
[37] a) G. K. Moortgat, H. Meyrahn, P. Warneck, *Chemphyschem* **2010**, *11*, 3896-3908; b) M. F. Shaw, B. Sztaray, L. K. Whalley, D. E. Heard, D. B. Millet, M. J. T. Jordan, D. L. Osborn, S. H. Kable, *Nature Comm.* **2018**, *9*.
[38] a) I. Mazzarino, P. Piccinini, L. Spinelli, *Catal. Today* **1999**, *48*, 315-321; b) A. W. Harrison, M. F. Shaw, W. J. De Bruyn, *J. Phys. Chem. A* **2019**, *123*, 8109-8121.
[39] A. M. Deal, B. N. Frandsen, V. Vaida; 2021; Data set for "Lactic Acid Photochemistry Following Excitation of S0 to S1 at 220 to 250 nm" in JPOC; CU Scholar; 10.25810/tg1y-3a80

[39]

Table 1: Calculated lactic acid relative abundance and associated vertical excitation energy (VEE) for the four most abundant conformers in the gas phase. Vertical excitation energies (reported in eV and nm) and associated oscillator strengths (unitless) are calculated for electronic transitions from the ground state, S_0, to the first singlet excited state, S_1.

Conformer	Relative abundance %, Ref [15a]/This work[a]	$S_0 \rightarrow S_1$ VEE, eV/nm (Oscillator strength)[b]	$S_0 \rightarrow S_1$ VEE, eV/nm (Oscillator strength)[c]
SsC	94.0/93.6	6.14/201.8 ($6*10^{-4}$)	6.15/201.7 ($4*10^{-4}$)
GskC	2.8/2.6	5.75/215.8 ($9*10^{-4}$)	5.80/213.9 ($5*10^{-4}$)
G'sk'C	2.0/2.0	5.76/215.1 ($24*10^{-4}$)	5.85/211.8 ($13*10^{-4}$)
AaT	1.1/1.6	5.86/211.5 ($6*10^{-4}$)	5.90/210.1 ($5*10^{-4}$)

[a]Based on ωB97X-D/aug-cc-pVTZ calculated Gibbs energies.
[b]TD-DFT at the ωB97X-D/aug-cc-pVTZ level, using geometries optimized at the same level.
[c]Calculated at the EOM-CCSD/6-311+G(d) level with CCSD/6-311+G(d) optimized geometries.

Table 2: Calculated aqueous relative abundances, vertical excitation energies (VEE), and relative excitation rates (ER) for each lactic acid conformer considered in this work. Vertical excitation energies (reported in eV and nm) and associated oscillator strengths (unitless) are calculated for electronic transitions from the ground state, S_0, to the first singlet excited state, S_1. These results are from ωB97X-D/aug-cc-pVTZ calculations with simulated water solvation using a PCM model.

Conformer	Relative abundance %[15a]	$S_0 \rightarrow S_1$ VEE, eV/nm (Oscillator strength)	Relative ER %
SsC	52.4	6.21/199.9 ($8*10^{-4}$)	38.9
GskC	6.5	5.85/211.8 ($7*10^{-4}$)	8.6
G'sk'C	2.9	5.83/212.8 ($25*10^{-4}$)	14.7
AaT	33.1	5.88/210.9 ($5*10^{-4}$)	29.8
AsC	2.2	6.01/206.5 ($11*10^{-4}$)	3.3
SsT	1.5	6.18/200.7 ($13*10^{-4}$)	1.9
AaC	1.3	6.01/206.5 ($16*10^{-4}$)	2.8